INTERNATIONAL JOURNAL FOR NUMERICAL AND ANALYTICAL METHODS IN GEOMECHANICS
Int. J. Numer. Anal. Meth. Geomech. 2012; **36**:391–421
Published online 23 March 2011 in Wiley Online Library (wileyonlinelibrary.com). DOI: 10.1002/nag.1011

THM analysis of a large-scale heating test incorporating material fabric changes

Marcelo Sánchez[1,*,†], Antonio Gens[2] and Sebastiá Olivella[2]

[1]*Zachry Department of Civil Engineering, Texas A&M University, College Station, TX, U.S.A.*
[2]*Department of Geotechnical Engineering and Geosciences, Universitat Politècnica de Catalunya (UPC), Barcelona, Spain*

SUMMARY

Engineered barriers are basic elements in the design of repositories for the isolation of high-level radioactive waste. This paper presents the thermo-hydro-mechanical (THM) analysis of a clay barrier subjected to heating and hydration. The study focuses on an ongoing large-scale heating test, at almost full scale, which is being carried out at the CIEMAT laboratory under well-controlled boundary conditions. The test is intensely instrumented and it has provided the opportunity to study in detail the evolution of the main THM variables over a long period of time. Comprehensive laboratory tests carried out in the context of the FEBEX and NF-PRO projects have allowed the identification of the model parameters to describe the THM behaviour of the compacted expansive clay. A conventional THM approach that assumes the swelling clay as a single porosity medium has been initially adopted to analyse the evolution of the test. The model was able to predict correctly the global THM behaviour of the clay barrier in the short term (i.e. for times shorter than three years), but some model limitations were detected concerning the prediction of the long-term hydration rate. An additional analysis of the test has been carried out using a double structure model to describe the actual behaviour of expansive clays. The double structure model explicitly considers the two dominant pore levels that actually exist in the FEBEX bentonite and it is able to account for the evolution of the material fabric. The simulation of the experiment using this enhanced model provides a more satisfactory reproduction of the long-term experimental results. It also contributes to a better understanding of the observed test behaviour and it provides a physically based explanation for the very slow hydration of the barrier. Copyright © 2011 John Wiley & Sons, Ltd.

Received 15 May 2009; Revised 9 August 2010; Accepted 28 November 2010

KEY WORDS: engineered barrier; nuclear waste; fabric/structure of soils; coupled analysis; expansive soils; unsaturated porous medium; suction

1. INTRODUCTION

The conceptual design of repositories for high-level nuclear waste generally envisages the placing of radioactive waste canisters in either horizontal drifts or vertical large diameter boreholes excavated at great depths in suitable geological media. Canisters are surrounded by engineered barriers made up of compacted expansive clays. This clay-based isolation system has the multiple purpose of providing mechanical stability for the waste canister (by absorbing stresses and deformations); serving as a buffer around it; sealing discontinuities in the emplacement boreholes and drifts; and delaying the water flow from the host rock. The latter function is an important one, because it

*Correspondence to: Marcelo Sánchez, Zachry Department of Civil Engineering, Texas A&M University, College Station, TX, U.S.A.
†E-mail: msanchez@civil.tamu.edu

postpones the contact between water and the waste as long as possible. The time to reach the full saturation of the barrier is a key parameter due to its impact on the long-term performance of the system and on the repository lifetime.

The behaviour of the clay barrier is highly complex, since it involves coupled thermo-hydro-mechanical (THM) phenomena that take place due to the simultaneous heating (generated by the waste radioactive decay) and hydration of the barrier (due to inflow of water from the surrounding rock). The understanding of the main THM processes and their couplings requires the contribution of experimental and fundamental studies. In the last few years, several full-scale tests have been carried out aimed at advancing the current knowledge about the behaviour of this kind of a system and to demonstrate the feasibility of different conceptual designs [1–5]. They have been normally performed in underground research laboratories excavated in a variety of geological media in order to examine the interaction of the host rock with the engineered barrier. This implies that the results of the tests are affected by the unavoidable variability and complexity of a natural geological system.

There is, therefore, merit in performing large-scale tests under controlled laboratory conditions so that the THM behaviour of the engineered barrier can be observed under well-known initial and boundary conditions eluding the uncertainties of the natural system. This paper focuses on one such test: the 'FEBEX mock-up test' [6], an ongoing heating experiment, at almost full scale, performed in the premises of CIEMAT laboratory in Madrid, in the context of the European projects FEBEX (Full-scale Engineered Barriers Experiment [1]) FEBEX II and NF-PRO [7].

Because of the very low permeability of the bentonite, significant results require observations over very long periods of time. In this respect, the 'FEBEX mock-up test' is quite exceptional as the evolution of the main THM variables has been recorded since the start of the heating and hydration of the experiment on 11 February 1997, more than a decade ago. The experiment is intensively instrumented and most of the sensors (recording. temperature, heater power, relative humidity, water intake, total pressure, etc.) are still operational. A large amount of data have therefore been collected from perhaps the large-scale test with the longest duration without changes in the testing conditions.

The THM formulation proposed by Olivella *et al.* [8] and the corresponding computer code CODE_BRIGHT [9] have been used in this work to interpret and describe the behaviour of the clay barrier. The determination of the model parameters used in the analyses has been based on an extensive campaign of laboratory tests carried out during the FEBEX and NF-PRO projects. Application of conventional models to the analysis of the tests has revealed that the long-term observed behaviour departed from initial predictions, especially those related to the time required to reach the full saturation of the barrier. The work presented herein explores the potential role of clay-fabric changes during confined hydration to explain the unexpected barrier behaviour.

During hydration the clay fabric exhibits an evolving character [10–12] that may affect strongly the kinetics of hydration, especially if confined conditions prevail. Single porosity models are not able to tackle properly the role that different pore levels play during the hydration process of swelling clays. A more detailed analysis of the clay fabric effects in the evolution of the mock-up test has therefore been performed with the aid of a double structure model [13–15]. Using this concept, the effect of two dominant pore levels that typically exist in compacted expansive clays can be explicitly included in the analysis.

The paper is organized as follows: a short description of the mock-up test is presented first, followed by a brief introduction to the THM formulation and the main constitutive laws adopted in the analysis. Afterwards, the numerical analysis of the clay barrier evolution using a conventional model is presented and the differences between observations and predictions are identified. Information about the evolving fabric of the compacted clay is then introduced together with the double structure model used to represent it. The results of the numerical analysis using this enhanced model are then presented and discussed. Finally, the conclusions draw together the various aspects of the research presented. Additional information is presented in the Appendix. The meaning of the symbols used in this paper is listed in Table I.

DOI: 10.1002/nag

Table I. Notation.

α_G	parameter related to the plastic potential	$\mathbf{D}_{\mathrm{e}}$	elastic matrix
α_0	parameter for elastic thermal strain	$\mathbf{D}_{\mathrm{ep}}$	elasto-plastic matrix
α_1	parameter that relates p_0^* with T	$\mathbf{D}_\alpha^i$	dispersion tensor of the medium ($i=w,a;\alpha=l,g$)
α_2	parameter for elastic thermal strain	e	total void ratio
α_3	parameter that relates p_0^* with T	e_{M}	macrostructural level void ratio
α_{m}	parameter controlling the microstructural soil stiffness	e_{m}	microstructural level void ratio
β_{m}	parameter controlling the microstructural soil stiffness	F_{LC}	*BBM* yield surface
χ	parameter related to the degree of saturation of the macrostructure	f_β	interaction function related to the coupling between macro and micro levels
ΔT	temperature increment ($T-T_0$)	G	plastic potential
ε	strain vector $\{\varepsilon_x,\varepsilon_y,\varepsilon_z,\gamma_{xy},\gamma_{xz},\gamma_{yz}\}^T$	G_t	shear modulus
$\dot{\varepsilon}^{\mathrm{e}}$	elastic strain increment due to stress changes	g	a lode angle function
$\dot{\varepsilon}_{\mathrm{s}}^{\mathrm{e}}$	elastic strain increment due to suction changes	$\mathbf{I}$	identity matrix
$\dot{\varepsilon}_{\mathrm{T}}^{\mathrm{e}}$	elastic strain increment due to temperature changes	$\mathbf{i}_\alpha^i$	non-advective mass flux ($i=w,a;\alpha=l,g$)
$\varepsilon_{\mathrm{vm}}$	elastic volumetric strain at microstructural level	$\mathbf{i}_c$	non-advective heat flux
$\varepsilon_{\mathrm{v}}^{\mathrm{p}}$	total plastic volumetric strain	J	second stress invariant of deviatoric stress tensor
$\varepsilon_{\mathrm{LC}}^{\mathrm{p}}$	plastic volumetric strain related to the yielding of the *LC*	$\mathbf{j}_{E\alpha j}$	advective energy flux in α phase with respect to a fixed reference system
κ	macrostructural elastic stiffness parameter for changes in mean stress	$\mathbf{j}_\alpha^i$	total mass flux of i-species in α phase with respect to a fixed reference system
κ_s	macrostructural elastic stiffness parameter for changes in suction	K	global bulk modulus
κ_{m}	parameter controlling the microstructural soil stiffness	K_{s}	macrostructural bulk modulus for changes in suction
λ	thermal conductivity	K_{T}	macrostructural bulk modulus for changes in temperature
$\lambda_{(s)}$	macrostructural compressibility parameter for changes in net mean stress for virgin states of soil at suction s	K_{M}	macrostructural bulk modulus for changes in mean stress
$\lambda_{(s)}$	macrostructural compressibility parameter for changes in net mean stress for virgin states of soil at suction s	K_{m}	microstructural bulk modulus for changes in mean stress plus suction
λ_0, λ_d	retention curve parameters	k_0	the intrinsic permeability at a reference porosity
λ_{LC}	plastic multiplier related to the *BBM*	b	model parameter intrinsic permeability
μ	poisson's coefficient	k	parameter describing the increase in cohesion with suction
μ_α	dynamic viscosity of α phase ($\alpha=l,g$)	LC	Loading–Collapse yield surface (BBM)
θ	Lode's angle	n	porosity
θ_α^i	($=\rho_\alpha\omega_\alpha^i$ mass of i-species in α phase per unit volume of α phase ($i=w,a;\alpha=l,g$)	$\hat{p}$	microstructural effective stress
ω_α^i	mass fraction of i-species in α phase ($i=w,a;\alpha=l,g$)	p	mean net stress
ρ	parameter that relates cohesion and T	p_c	reference stress
ρ_{s}	solid density	p_0	net mean yield stress at current suction and temperature
ρ_α	mass of α phase per unit of volume of α phase ($\alpha=l,g$)	p_0^*	net mean yield stress for saturated conditions at reference temperature
$\boldsymbol{\sigma}_t$	total stress vector. $\{\sigma_x,\sigma_y,\sigma_z,\tau_{xy},\tau_{xz},\tau_{yz}\}_t^T$	p_{0T}^*	net mean yield stress for saturated conditions at current temperature
$\boldsymbol{\sigma}$	net stress vector ($\boldsymbol{\sigma}_t-\mathbf{I}p_g$)	p_r	reference stress

DOI: 10.1002/nag

Table I. *Continued.*

ζ	parameter controlling the rate of increase of macrostructural soils stiffness with suction	P_0, P_d	retention curve parameters
	Acronyms	q_α	volumetric flux of α phase with respect to the solid ($\alpha = l, g$)
BBM	Barcelona Basic Model	r	parameter defining the minimum macrostructural soil compressibility
Dou	Double structure case	s	matric suction ($p_g - p_l$)
OBC	Operational Base Case	S_α	volumetric fraction of pore volume occupied by α phase ($\alpha = l, g$)
THM	Thermo-hydro-mechanical	T	temperature (T_0 = reference temperature)

2. FEBEX MOCK-UP TEST

The mock-up test is still being carried out at the CIEMAT laboratory in Madrid. The aim of the FEBEXs and NF-PRO projects has been to study the behaviour of the barrier components in the near-field of a high-level radioactive waste repository in crystalline rock (granite). The experiment is based on the Spanish disposal reference concept, which considers the waste canister placed horizontally in drifts and surrounded by a clay barrier constructed from highly compacted bentonite blocks. The experimental study is composed of three main parts [1]: (i) an *in situ* test under natural conditions and at full scale [5]; (ii) a mock-up test at almost full scale and (iii) a series of laboratory tests to complete the information from the two large-scale tests.

The *in situ* test operates under natural conditions at the underground laboratory managed by NAGRA, at the Grimsel test site in Switzerland. The mock-up test is performed at the CIEMAT laboratory in Madrid under well-controlled initial and boundary conditions. A controlled temperature room was built to host the mock-up test. The physical components of the mock-up test consist of five basic units: the confining structure with its hydration system, the clay barrier, the instrumentation, and the system for data acquisition and for heater control. Figure 1(a) shows a picture of the mock-up test and Figure 1(b) presents a schematic representation of the experiment.

The confining structure is a cylindrical steel body with a useful length of 6.00 m and an inner diameter of 1.62 m. The hydration system supplies water under pressure to the periphery of the clay barrier. To simulate the water that saturates the barrier in a repository excavated in granitic rock 'granitic water' was injected. The granitic water has a salinity of 0.02% and a pH of 8.3, more details about the chemistry of the injected water can be found elsewhere [1]. A flexible geotextile has been placed around the outer boundary of the barrier to ensure uniform hydration conditions. The main elements of the heating system are two heaters located concentrically in the confining structure. The clay barrier is formed from highly compacted blocks of FEBEX bentonite. The blocks were fabricated with an average water content of 13.6% and the average dry density of the barrier is 1.65 mg/m^3. The instrumentation includes sensors installed in the clay barrier, in the heaters and in the confining structure. The main measured variables are: temperature, relative humidity, fluid pressure and total pressure. Figure 2 shows the monitored cross sections and the positions of the different sensors in each of those sections.

The main characteristics of the test can be summarized as: (i) the test has a clay barrier with an unlimited availability of hydration water, supplied at constant and controlled pressure; (ii) the mass of water introduced into the system is continuously measured and recorded; (iii) the boundary conditions are well-defined and controlled; (iv) the initial conditions are well established at the beginning of the heating phase; (v) the test is intensively instrumented, with several sensors located along the barrier which register the evolution of the main THM variables and (vi) the experiment has two electrical heaters, symmetrically placed in relation to the central section of the test. Therefore, the measurements made in sections located symmetrically with respect to the central section should be much the same. This provides an excellent way to check on the repeatability and reliability of the observations.

DOI: 10.1002/nag

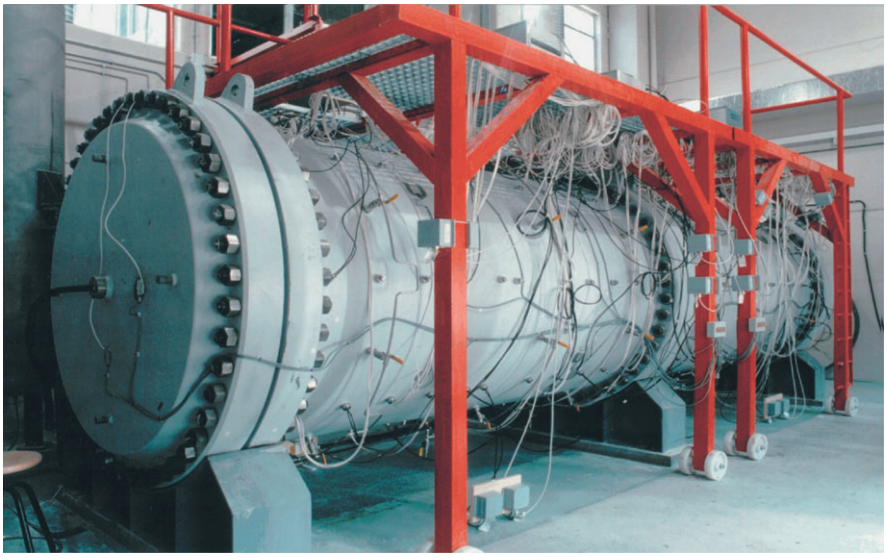

(a)

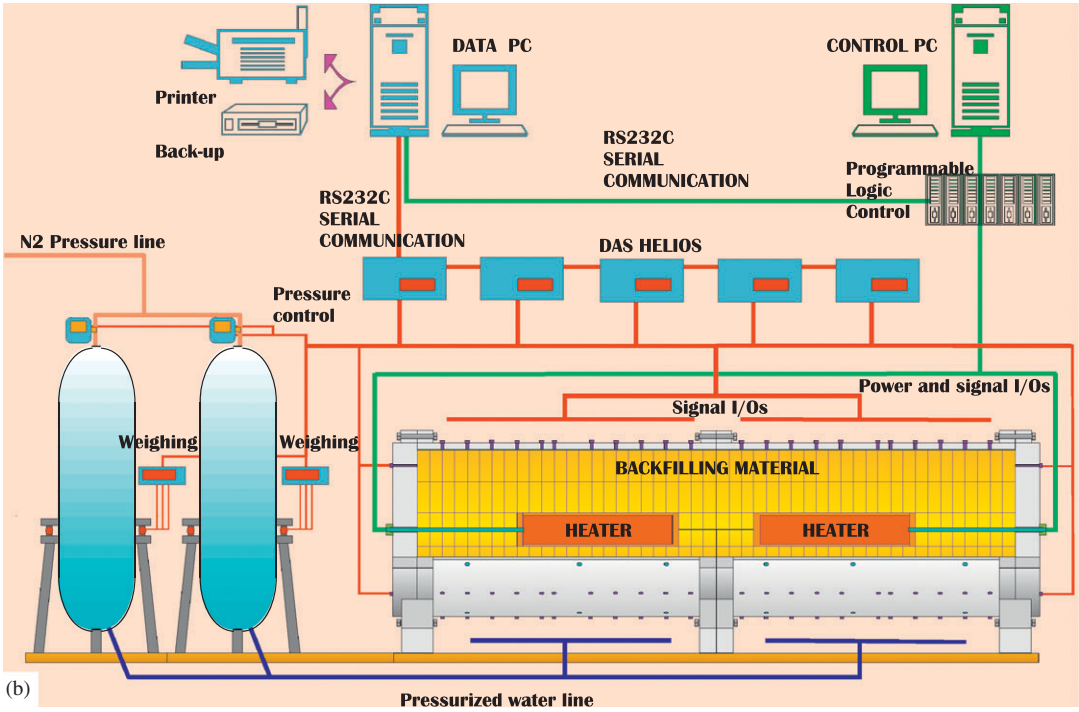

(b)

Figure 1. (a) Mock-up test and (b) schematic representation of the main components of the experiment.

3. THM FORMULATION

Several strongly coupled THM phenomena take place when an unsaturated clay barrier is submitted to simultaneous heating and hydration. Although they have been qualitatively described elsewhere [5, 16], they are briefly considered here for completeness. For example, hydration takes place from the external boundary inwards driven by the gradient between the applied water pressure and the suction in the bentonite. Hydration will cause a progressive rise in the degree of saturation. This affects both the temperature field, due to the modifications of thermal conductivity, and the stress-strain distribution, due to suction changes. On the other hand, in the inner part of the buffer,

DOI: 10.1002/nag

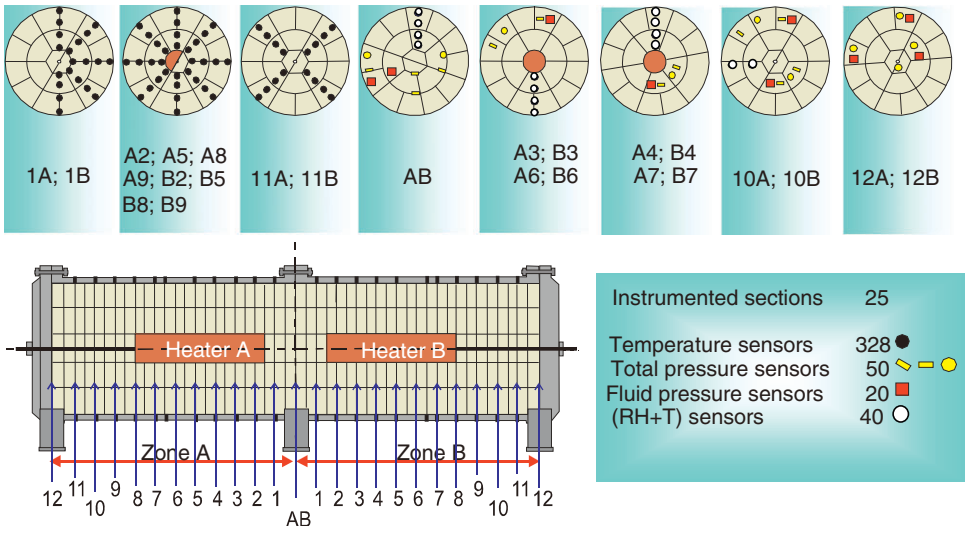

Figure 2. Mock-up test: instrumented sections, sensors types and positions in zones A and B of the barrier.

applied heat causes a temperature rise that moves outwards with time. Temperature-induced water evaporation causes drying of the bentonite. Vapour coming from the inner part of the barrier will diffuse towards the outer regions where it will condense causing a local rise of the degree of saturation. Water transfer is also affected by the dependence of water viscosity on temperature and by porosity changes arising from variations in stresses and suction. The analysis of this type of a problem requires a formal and consistent framework.

The theoretical framework used to analyse the problem is the coupled THM formulation proposed in [8], extended to consider clayey materials. The approach is composed of three main parts: balance equations, constitutive equations and equilibrium restrictions. The framework is formulated using a multi-phase, multi-species approach. The subscripts identify the phase ('s' for solid, 'l' for liquid and 'g' for gas). The superscript indicates the species ('h' for mineral, 'w' for water and 'a' for air). The liquid phase may contain water and dissolved air, and the gas phase may be a mixture of dry air and water vapour. Dry air is considered as a single species. A brief account of the formulation is included below; a detailed description can be found elsewhere [5, 8, 9, 16].

3.1. Balance equations

Mass balance equations were established following the compositional approach, which consists of balancing the species rather than the phases. Water is present in liquid and gas phases. The total mass balance of water is expressed as

$$\frac{\partial}{\partial t}(\theta_l^{\mathrm{w}} S_{\mathrm{l}} n + \theta_{\mathrm{g}}^{\mathrm{w}} S_{\mathrm{g}} n) + \nabla \cdot (\mathbf{j}_{\mathrm{l}}^{\mathrm{w}} + \mathbf{j}_{\mathrm{g}}^{\mathrm{w}}) = f^{\mathrm{w}} \tag{1}$$

where $\theta_{\mathrm{l}}^{\mathrm{w}}$ and $\theta_{\mathrm{g}}^{\mathrm{w}}$ are the masses of water per unit volume of liquid and gas, respectively; n is the porosity; S_{l} and S_{g} represent the volumetric fraction of pore volume occupied by liquid and by gas (degree of saturation for their respective phases) and $\mathbf{j}_{\mathrm{l}}^{\mathrm{w}}$ and $\mathbf{j}_{\mathrm{g}}^{\mathrm{w}}$ denote the total mass fluxes of water in the liquid and gas phases (water vapour), with respect to a fixed reference system. f^{w} is an external supply of water. The main variable associated with this equation is the liquid pressure (P_{l})[9]. Similarly for the air

$$\frac{\partial}{\partial t}(\theta_{\mathrm{l}}^{\mathrm{a}} S_{\mathrm{l}} n + \theta_g^{\mathrm{a}} S_{\mathrm{g}} n) + \nabla \cdot (\mathbf{j}_{\mathrm{l}}^{\mathrm{a}} + \mathbf{j}_{\mathrm{g}}^{\mathrm{a}}) = f^{\mathrm{a}} \tag{2}$$

where $\theta_{\mathrm{a}}^{\mathrm{l}}$ and $\theta_{\mathrm{a}}^{\mathrm{g}}$ are the masses of air per unit volume of liquid and gas phases, respectively. $\mathbf{j}_{\mathrm{l}}^{\mathrm{a}}$ and $\mathbf{j}_{\mathrm{g}}^{\mathrm{a}}$ denote the total mass fluxes of air in the liquid and gas phases with respect to a fixed reference

DOI: 10.1002/nag

system. f^{a} is the external mass supply of air per unit volume of medium. The gaseous phase is assumed as a mixture of air and water vapour and the gas pressure (P_g) is the main variable associated with this equation.

Thermal equilibrium between phases is assumed. This hypothesis means that at a given material point, the three phases (i.e. solid, liquid and gas) are at the same temperature and, consequently, only one equation is required to establish the energy balance. This hypothesis is justified considering the low permeability of the expansive clays. The total internal energy per unit volume of porous media is obtained adding the internal energy of each phase corresponding to each medium. Applying the balance equation to this quantity, the following equation is obtained [8]:

$$\frac{\partial}{\partial t}(E_s\rho_s(1-n)+E_l\rho_l S_l n+E_g\rho_g S_g n)+\nabla\cdot(\mathbf{i}_c+\mathbf{j}_{Es}+\mathbf{j}_{El}+\mathbf{j}_{Eg})=f^{E} \tag{3}$$

where E_s is the solid-specific internal energy; E_l and E_g are specific internal energies corresponding to the liquid and gas phases, respectively; ρ_s is the solid density; ρ_l and ρ_g are the liquid and gas phase densities; $\mathbf{i}_c$ is the conductive heat flux; $\mathbf{j}_{Es}$ is the advective energy flux of solid phase with respect to a fixed reference system; $\mathbf{j}_{El}$ and $\mathbf{j}_{Eg}$ are the advective energy flux of liquid and gas phases, respectively, with respect to a fixed reference system and f^{E} is the energy supply per unit volume of medium.

The balance of momentum for the porous medium reduces to the equilibrium equation in total stresses:

$$\nabla\cdot\boldsymbol{\sigma}+\mathbf{b}=0 \tag{4}$$

where $\boldsymbol{\sigma}$ is the stress tensor and $\mathbf{b}$ is the vector of body forces. Through an adequate constitutive model (presented in the next section), the equilibrium equation is transformed into a form expressed in terms of solid velocities and fluid pressures. The assumption of small strain rate is also made. The displacement field ($\mathbf{u}$) is the main variable associated with this equation [9]. In addition, the mass balance of solid is established for the whole porous medium and it is used to update the porosity [8, 9].

3.2. Constitutive equations and equilibrium restrictions

The constitutive equations establish the link between the main unknowns (e.g. displacements, fluid pressures and temperature) and the dependent variables (e.g. stresses and degree of saturation).

Mechanical model. The Barcelona Basic Model (BBM) has been initially adopted to model the mechanical behaviour of the clay barrier [17]. The BBM is an elasto-plastic strain hardening model, which extends the concept of critical state for saturated soils to the unsaturated conditions and it is able to reproduce many of the basic patterns of behaviour observed in unsaturated soils. The BBM considers two independent stress variables: the net stress ($\boldsymbol{\sigma}$) computed as the excess of the total stresses over the gas pressure ($\boldsymbol{\sigma}_t-\mathbf{I}p_g$), and the matric suction (s), computed as the difference between gas pressure and liquid pressure. The model is formulated in terms of the three stress invariants (p; J; θ); suction and temperature (the invariants are defined in the Appendix). In the BBM the yield surface depends also on the matric suction (Figure 3). The trace of the yield function on the isotropic $p-s$ plane is called the LC (Loading–Collapse) yield curve, because it represents the locus of activation of irreversible deformations due to loading increments or wetting (collapse compression). The position of the LC curve is given by the value of the hardening variable p_0^*, which is the apparent pre-consolidation yield stress of the saturated state. The ideas proposed in [18] have been adopted to extend the BBM to non-isothermal condition, considering that thermal changes affect both elastic and plastic behaviour. Pre-consolidation pressure is affected by the temperature assuming that temperature increases reduce the size of the yield surface and the strength of the material. This is a well-established behaviour for saturated conditions [19], and it can also be extended to the unsaturated conditions, as confirmed in the recent experimental studies

DOI: 10.1002/nag

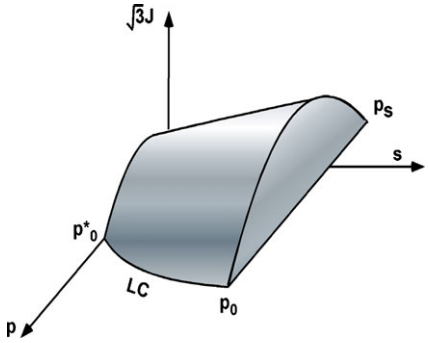

Figure 3. 3-D representation of the Barcelona Basic Model yield surface, including the LC (Loading Collapse yield curve), p_0^* (the history variable of the model), p_0 and p_s.

Table II. Model parameters related to BBM.

κ	0.04	κ_s	0.25
v	0.4	α_{is}	−0.003
α_{sp}	−0.147	α_{ss}	0.00
α_0	$1.5\times10^{-4}(^\circ\mathrm{C}^{-1})$	α_2	0.00
λ_0	0.15	p_c	0.10 MPa
p_0^*	14 MPa	α	0.395
r	0.75	β	0.05
M	1.5	T_0	20°C
k	0.1	ρ	0.2

[20, 21]. The BBM yield surface (F_{LC}) is then expressed as

$$F_{\mathrm{LC}}=3J^2-\left[\frac{g(\theta)}{g(-30^\circ)}\right]^2 M^2(p+p_s)(p_0-p)=0 \tag{5}$$

where M is the slope of the critical state, p_0 is the apparent unsaturated isotropic pre-consolidation pressure at a specific value of suction and p_s considers the dependence of shear strength on suction and temperature. To complete the definition of the yield surface as set out in (5) it is necessary to adopt a suitable Lode's angle function, $g(\theta)$.

When yielding takes place the increment of plastic deformations is evaluated through

$$\dot{\varepsilon}^{\mathrm{p}}_{\mathrm{LC}}=\lambda_{\mathrm{LC}}\frac{\partial G}{\partial \boldsymbol{\sigma}} \tag{6}$$

where λ_{LC} is the plastic multiplier and G is the plastic potential (defined in the Appendix).

The hardening law is expressed as a rate relation between the volumetric plastic strain and the saturated isotropic pre-consolidation stress 'p_0^*' (Figure 3), according to

$$\frac{\dot{p}_0^*}{p_0^*}=\frac{(1+e)}{(\lambda_{(0)}-\kappa)}\dot{\varepsilon}^{\mathrm{p}}_{\mathrm{v}} \tag{7}$$

where e is the void ratio, $\varepsilon_{\mathrm{v}}^{\mathrm{p}}$ is the volumetric plastic strain, κ is the elastic compression index for changes in p, evaluated through Equation 8(a) and $\lambda_{(0)}$ is the stiffness parameter for changes in p for virgin states of the soil in saturated condition.

The yield surface associated with suction increase proposed in the original version of the BBM [17] is not considered in this analysis. Owing to the high compaction to which the bentonite blocks have been subjected, the description of the behaviour of the material inside the yield surface is particularly important. According to the adopted parameters (Table II), it is expected that the

DOI: 10.1002/nag

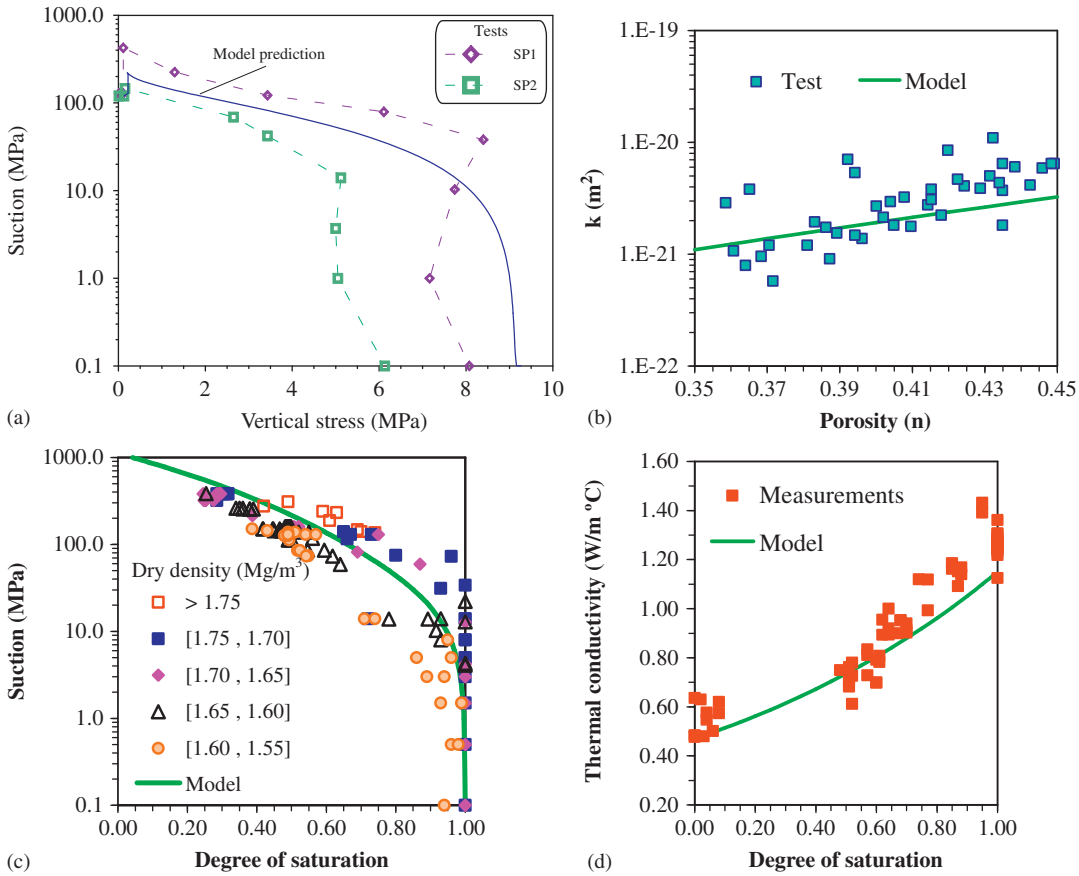

Figure 4. Main constitutive laws. (a) Mechanical: computed stress path for swelling pressure tests using the BBM. Experimental results (SP1 and SP2 paths) are provided for comparison. (b) Hydraulic: variation of saturated permeability with porosity. Experimental data and adopted model for the intrinsic permeability law. (c) Hydraulic: retention curve adopted in the analyses, together with the experimental data for FEBEX bentonite (symbols). (d) Thermal: Thermal conductivity: FEBEX bentonite experimental results (symbols) and model fitting.

whole stress path will lie inside the BBM yield surface. The variation of stress-stiffness with suction and the variation of swelling potential with stress and suction have been considered [22]. The resulting elastic model is the following:

$$\dot{\varepsilon}_v^e = \frac{\kappa}{(1+e)}\frac{\dot{p}}{p} + \frac{\kappa_s}{(1+e)}\frac{\dot{s}}{(s+0.1)} + (\alpha_0 + \alpha_2 \Delta T)\dot{T} \quad \text{(a)}; \quad \dot{\varepsilon}_s^e = \frac{\dot{J}}{G_t} \quad \text{(b)} \tag{8}$$

where κ_s is the macrostructural elastic stiffness parameter for changes in suction, G_t is the shear modulus; α_0 and α_2 are model parameters related to temperature [18]. κ, κ_s and G_t are evaluated according to

$$\kappa = \kappa_i(1+\alpha_s s) \quad \text{(a)}; \quad \kappa_s = \kappa_{s0}(1+\alpha_{sp}\ln p/p_{\text{ref}}) \quad \text{(b)}; \quad G_t = \frac{3(1-2\mu)K}{2(1+\mu)} \quad \text{(c)} \tag{9}$$

where μ is the Poisson's coefficient; α_s and α_{sp} are model parameters [22] and the bulk modulus (K) is obtained from (A5), see Appendix. The parameters of the mechanical model are summarized in Table II. They were determined from the experimental laboratory campaign carried out during the FEBEX project [1]. As an example, Figure 4(a) shows the results of two swelling pressure tests (SP1 and SP2) [23], used for the experimental calibration of the model, together with the stress path computed with the model.

DOI: 10.1002/nag

Hydraulic models. Advective fluxes are computed using a generalized Darcy's law, expressed as [16]

$$\mathbf{q}_\alpha = -\mathbf{K}_\alpha(\nabla P_\alpha - \rho_\alpha \mathbf{g}); \quad \alpha = l, g \tag{10}$$

where P_α is the phase pressure. $\mathbf{K}_\alpha$ is the permeability tensor of α phase and $\mathbf{g}$ is the gravity vector. The permeability tensor is evaluated according to

$$\mathbf{K}_\alpha = \mathbf{k}\frac{k_{r\alpha}}{\mu_\alpha}; \quad \alpha = l, g \tag{11}$$

where $\mathbf{k}$ is the intrinsic permeability tensor, μ_α is the dynamic viscosity of the α phase and $k_{r\alpha}$ is the phase relative permeability. The dependence of intrinsic permeability on porosity has been based on Kozeny's law

$$\mathbf{k} = k_0 \frac{n^3}{(1-n)^2}\frac{(1-n_0)^2}{n_0^3}\mathbf{I} \tag{12}$$

where k_0 is the reference saturated permeability at the reference porosity n_0. Permeability tests performed on saturated samples have been used to adopt the reference values: $k_0 = 1.9 \times 10^{-21}\,\mathrm{m}^2$ for a porosity of 0.40 (Figure 4(b)).

The well-known power law has been adopted to describe the dependence of liquid permeability on the degree of saturation

$$k_{rl} = S_l^{n_s} \tag{13}$$

A value of $n_s = 3$ has been determined from back-calculating hydration tests on FEBEX bentonite [24]. As for the gas relative permeability law, the following model has been adopted:

$$k_{rg} = A(1 - k_{rl}) \tag{14}$$

For FEBEX bentonite, differences close to 7 orders of magnitude have been measured between water and gas intrinsic permeabilities [25]. As discussed in Olivella and Gens [26], if the value of intrinsic permeability for water is used in the analysis, the gas permeability obtained is several orders of magnitude smaller than the actual values. In order to maintain the concept of intrinsic permeability and until more experimental information became available, a correction has been applied to the relative permeability law, adopting a value of 'A' large enough (close to 1.0×10^7) to ensure a gas mobility in the FEBEX bentonite close to the values of gas permeability measured in the laboratory tests.

The water retention curve relates the degree of saturation of the material with suction. The law adopted is based on the van Genuchten model [27], as follows:

$$S_l = \left[1 + \left(\frac{s}{P_0}\right)^{\frac{1}{1-\lambda_0}}\right]^{-\lambda_0} f_d \quad \text{(a)}; \quad f_d = \left(1 - \frac{s}{P_d}\right)^{\lambda_d} \text{(b)} \tag{15}$$

where P_0 and λ_0 are model parameters. The function f_d is included in order to model properly the high suction range. Similar functions were proposed previously [28]. P_d is related with the suction at 0 degree of saturation and λ_d is a model parameter. When $\lambda_d = 0$ the model adopted in [18] is recovered. Figure 4(c)) presents the results of tests carried out at conditions of constant volume on FEBEX bentonite [1, 29], alongside the adopted model is presented. Model parameters are $P_0 = 20$ MPa; $\lambda_0 = 0.18$, $P_d = 1100$ MPa and $\lambda_d = 1.10$.

The relation between P_0 and surface tension (σ) suggested in [8] has been applied to this model. The change of P_0 in accordance with the following expression introduces a dependence of the retention curve with temperature

$$P_0 = P_{T_0}\frac{\sigma_T}{\sigma_{T_0}} \quad \text{(a)}; \quad \sigma_T = 0.03059 \exp\left(\frac{252.93}{273.15 + T}\right) \quad \text{(b)} \tag{16}$$

DOI: 10.1002/nag

For a given degree of saturation, this law predicts a small decrease in suction when temperature increases, consistent with observations made in laboratory tests [1, 29].

Non-advective fluxes of species inside the fluid phases are computed through Fick's law, which expresses them in terms of gradients of mass fraction of species through a hydrodynamic dispersion tensor that includes both molecular diffusion and mechanical dispersion:

$$\mathbf{i}_\alpha^i = -\mathbf{D}_\alpha^i \nabla \omega_\alpha^i \quad i = w, a; \quad \alpha = l, g \tag{17}$$

where $\mathbf{D}_\alpha^i$ is the dispersion tensor of the medium; a more detailed description of the adopted hydraulic models can be found elsewhere [8, 9].

Thermal model. Fourier's law has been adopted to describe the conductive flux of heat (Equation 18(a)). The thermal conductivity (λ) depends on the saturation of the clay and is expressed by the geometric mean of the thermal conductivities of the components (Equation 18(b)):

$$\mathbf{i}_c = -\lambda \nabla T \quad \text{(a)}; \quad \lambda = \lambda_{\text{sat}}^{S_l} \lambda_{\text{dry}}^{(1-S_l)} \quad \text{(b)} \tag{18}$$

Based on experimental results (Figure 4(d)), the following thermal conductivities have been adopted: $\lambda_{\text{dry}} = 0.47$ and $\lambda_{\text{sat}} = 1.15$.

Equilibrium restrictions. It is assumed that phase changes are rapid in relation to the characteristic times typical of the problem under consideration. Hence, they can be considered in local equilibrium, giving rise to a set of equilibrium restrictions that must be satisfied at all times [8]. The vapour concentration in the gaseous phase is governed by the psychometric law [8] and the amount of air dissolved in water is given by Henry's law [8].

4. THM MODELLING

The phase of heating and hydration of the test, known as the 'operational stage', started in February 1997 and is still ongoing at present. The numerical analysis presented in this section uses the conventional model outlined above that considers the bentonite as a single porosity medium. The analysis is called 'OBC' (Operational Base Case). In the following sections, a brief description of the main results of the 'OBC' model is presented with the objective of interpreting the main trends of the THM behaviour observed in the mock-up test. The experimental results have been supplied by CIEMAT, the data reported in this paper correspond until the day 18/06/2006 (day 3421).

All the analyses have been carried out using the computer program CODE_BRIGHT. Coupled analyses have been performed using a 2-D axisymmetric longitudinal section that includes the heaters, the bentonite barrier, the outer steel container and the geotextile between the barrier and the container (Figure 5(a)). Only one half of the problem is analysed because of symmetry. Experimental observations have then confirmed the properness of the idealization adopted in this modelling [6]. The mesh has 580 quadrilateral bilinear elements (Figure 5(b)) with four integration points. Selective integration according to [30] has been used.

4.1. Initial conditions

The initial global degree of the saturation of the mock-up test just before switching on the heaters was 71.50%. The same initial degree of saturation has been assumed in the model. An initially uniform temperature of 20°C is assumed in the entire domain. This is consistent with CIEMAT data [1]. As for the mechanical conditions, a hydrostatic value of 0.11 MPa has been adopted, approximately equal to the weight of the bentonite in the mid-diameter of the buffer.

4.2. Boundary conditions

Hydraulic boundary conditions. An applied water pressure of 0.55 MPa is applied in the geotextile (i.e. at the interface between steel and bentonite) in accordance with the actual test conditions.

DOI: 10.1002/nag

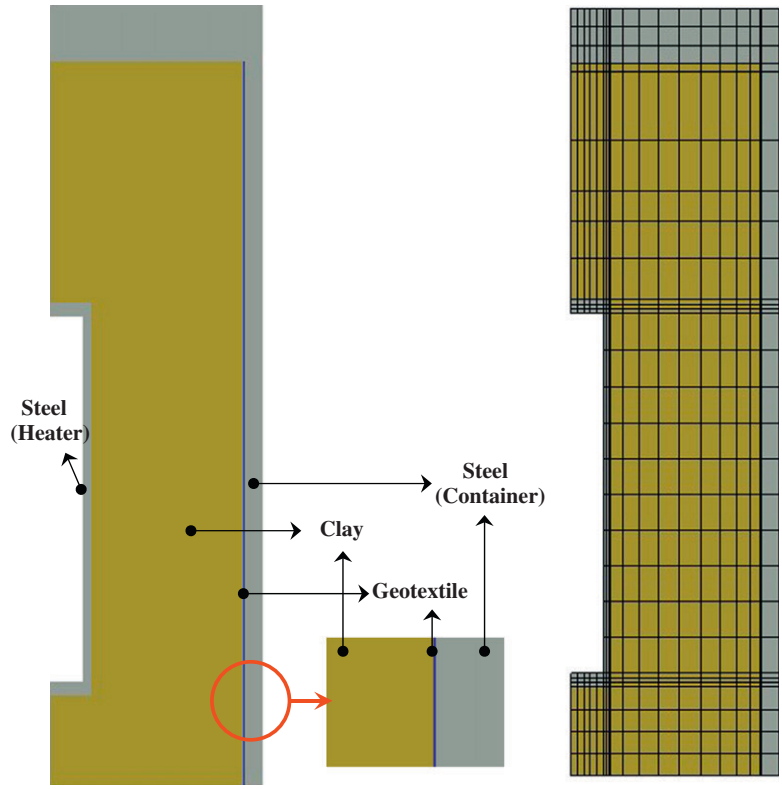

Figure 5. Axisymmetric geometry adopted for the analysis of the mock-up: (a) materials used in the modelling (no scale figure) and (b) model mesh.

Thermal boundary conditions. The thermal boundary conditions at a radius equal to 0.15 m (radial coordinate of the heater elements) reproduce testing conditions as follows:

(i) Day 0 to 6: constant power (250 W/heater);
(ii) Day 7 to t_{100}: constant power (500 W/heater);
(iii) t_{100} to the end of the test: constant temperature ($T = 100^\circ$C)

where t_{100} is the time at which the temperature reaches 100°C at some point in the bentonite (15.6 days for the analysis presented herein). On the external boundary, the following radiation condition has been applied:

$$j_e = \gamma_e (T^0 - T) \tag{19}$$

where j_e is the heat flow, T^0 is the prescribed temperature ($T^0 = 20^\circ$C) and γ_e is the radiation coefficient. A coefficient $\gamma_e = 5$ has been used.

Mechanical boundary conditions. For the outer boundary of the steel container, a stress-free condition has been prescribed. Note that the external steel cylinder is explicitly considered in the analysis, therefore strains and stresses are calculated by the computer code.

4.3. Results of the OBC analysis

The OBC analysis, reported in this section, corresponds to the modelling performed at the start of the test using the best information about test conditions and material parameters available at the time. The results cannot be considered strictly class A predictions because analysis and test overlapped for a few weeks at the beginning of the test. The main reason for the overlap is that the heating protocol was not totally defined at the start of the test but it was decided interactively

DOI: 10.1002/nag

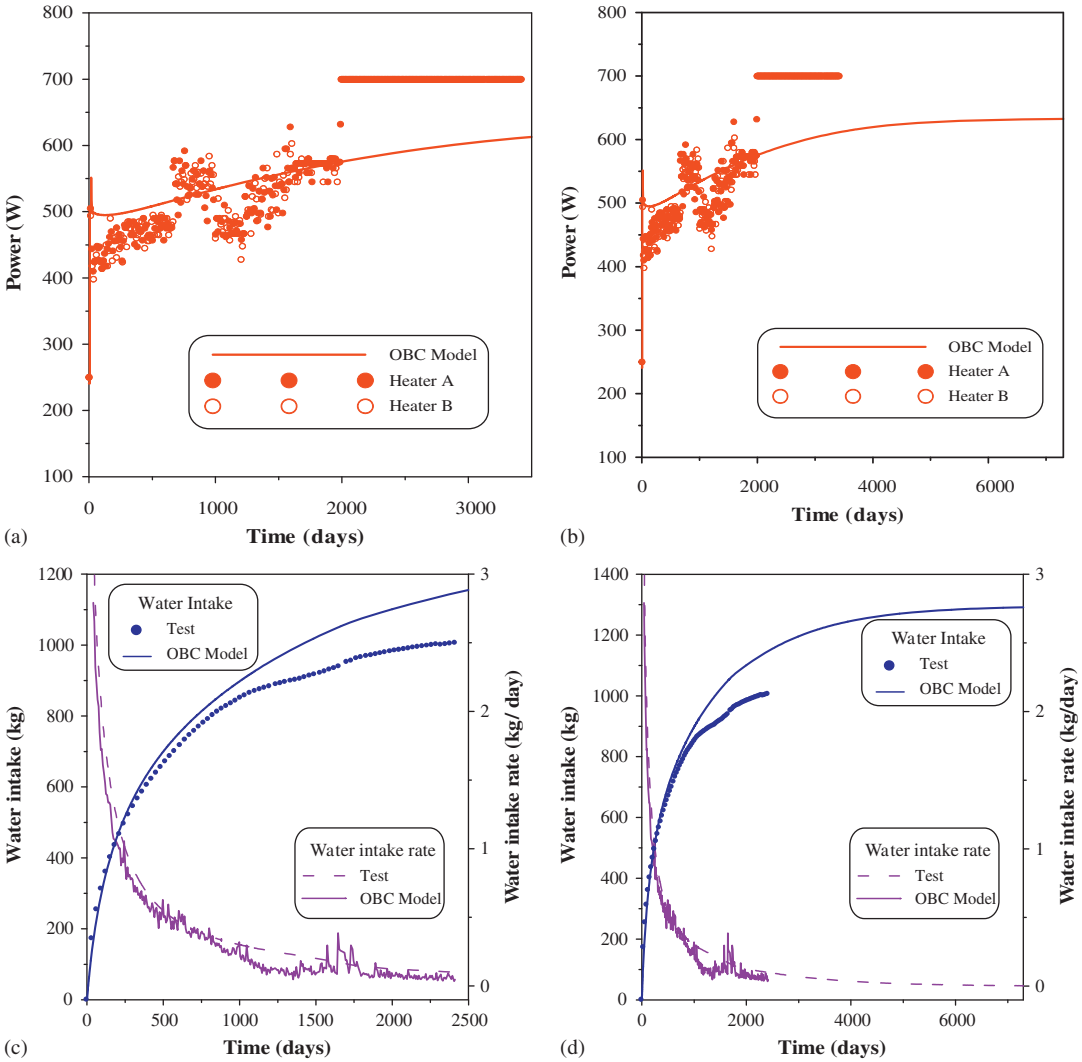

Figure 6. Evolution of global variables. (a) Evolution of heater power; observed and computed values (OBC model). (b) Evolution of heater power; long-term predictions (OBC model). (c) Evolution of water entry; observed and computed values (OBC model). (d) Evolution of water entry; long-term prediction (OBC model).

until reaching the desired temperature condition. In any case, the results of the OBC analysis are compared with the observations during a period of about 10 years; consequently the analysis results reported can be considered, to a very large extent, predictions.

The evolutions of the global variables of the problem (i.e. heater power and the water intake) are presented in Figure 6. Figures 7–9 show the time evolution of temperature, relative humidity and stresses at different points of the barrier. To illustrate the range of different patterns of bentonite behaviour, the comparisons between model computations and observations are centered on two characteristic cross sections: one identified as the 'hot cross section' (e.g. Sections A4 and B4, and Sections A5 and B5) is located in the heater area and the other one, called 'cool cross section' (e.g. Sections A10 and B10 and Sections A11 and B11), located away from the heater, in an area of quite small temperature increase. Results involving the other sections are presented in [31]. It should be noted that, in fact, the experimental observations of two symmetric instrumented sections are plotted. In a perfect test, they should yield the same results. Therefore, they readily provide a good check of the reliability of the sensors and of the tests performance.

DOI: 10.1002/nag

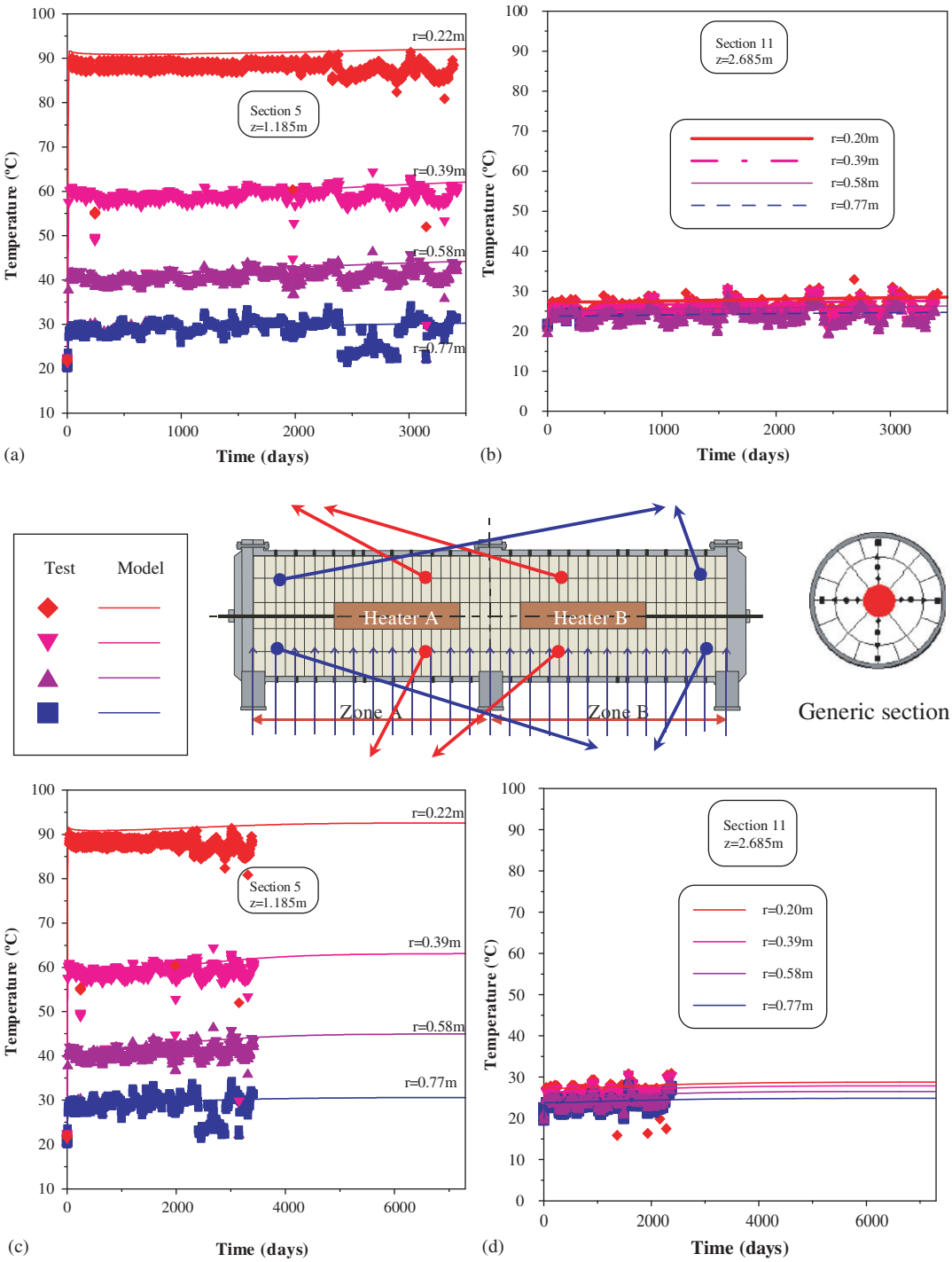

Figure 7. Evolution of temperature in the mock-up test. Observed versus computed values (OBC model). (a) Sections A5–B5 (hot cross section). (b) A11–B11 (cold cross section). (c) Sections A5–B5 long-term predictions. (d) Sections A11–11 long-term predictions.

Thermal results. The heaters are powered to provide a constant maximum temperature of 100° C at the contact between heaters and bentonite. The model yields good results regarding the thermal problem. This is reflected in the evolutions of the heater power (a global variable of the problem, Figure 6(a)), and in the comparisons of the model with local measures of temperatures

DOI: 10.1002/nag

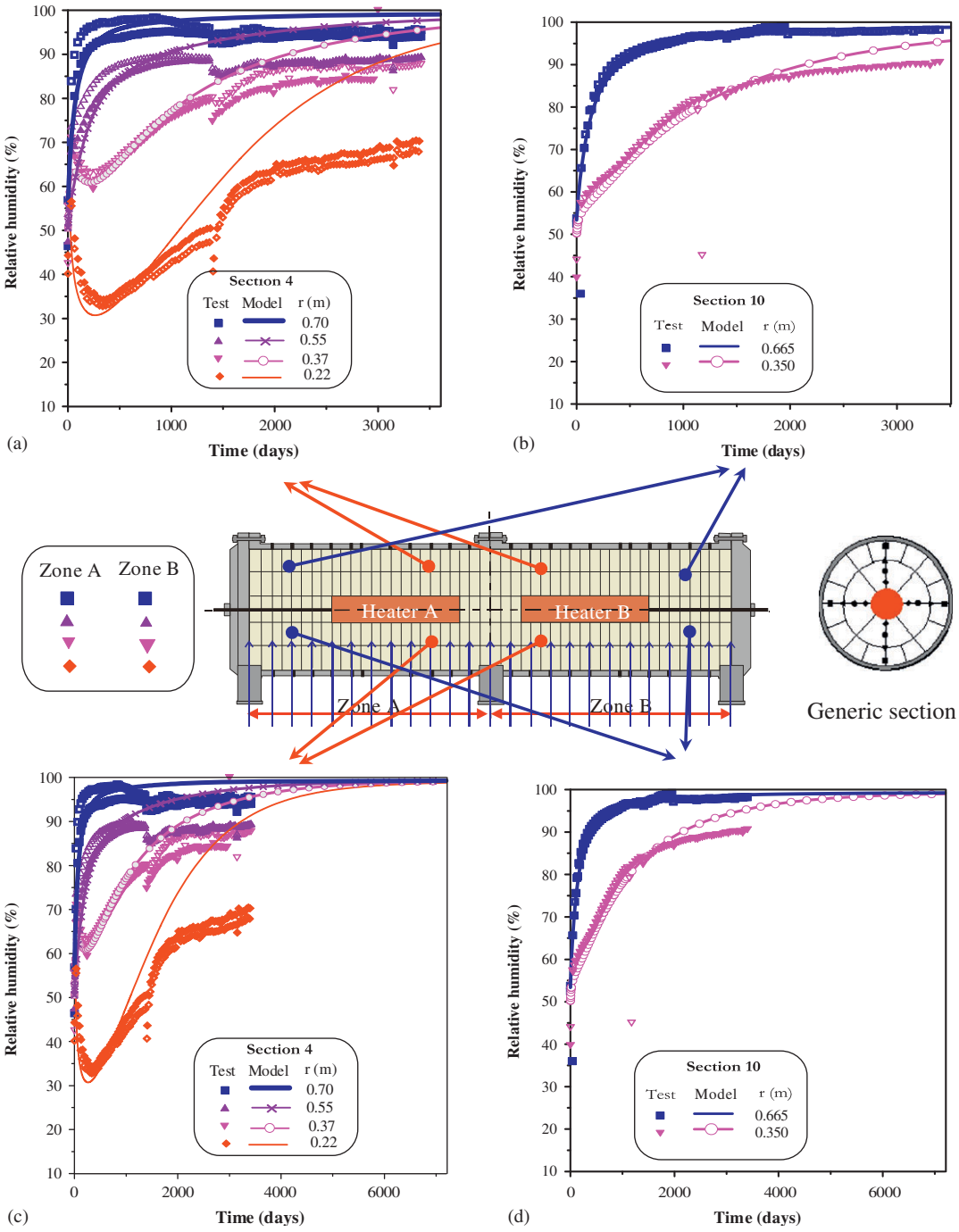

Figure 8. Evolution of relative humidity in the mock-up test. Observed versus computed values (OBC model). Bold symbols correspond to sensors in zone A, empty symbols correspond to sensors in zone B (Figure 2). (a) Sections A4–B4 (hot cross section). (b) A10–B10 (cold cross section). (c) Sections A4–B4 (long-term predictions). (d) Sections A10–B10 (long-term predictions).

(Figures 7(a) and (b)). It can be noted that there are some small differences in the temperature field, especially in zones close to the heater. They may be an effect of the lower thermal conductivity in the discontinuity that may exist between heater and bentonite, not considered in the analysis. The heater power predictions indicate a slow increment of the heater power (Figure 6(b)). This is a consequence of the progressive hydration of the bentonite barrier that causes an increase of

DOI: 10.1002/nag

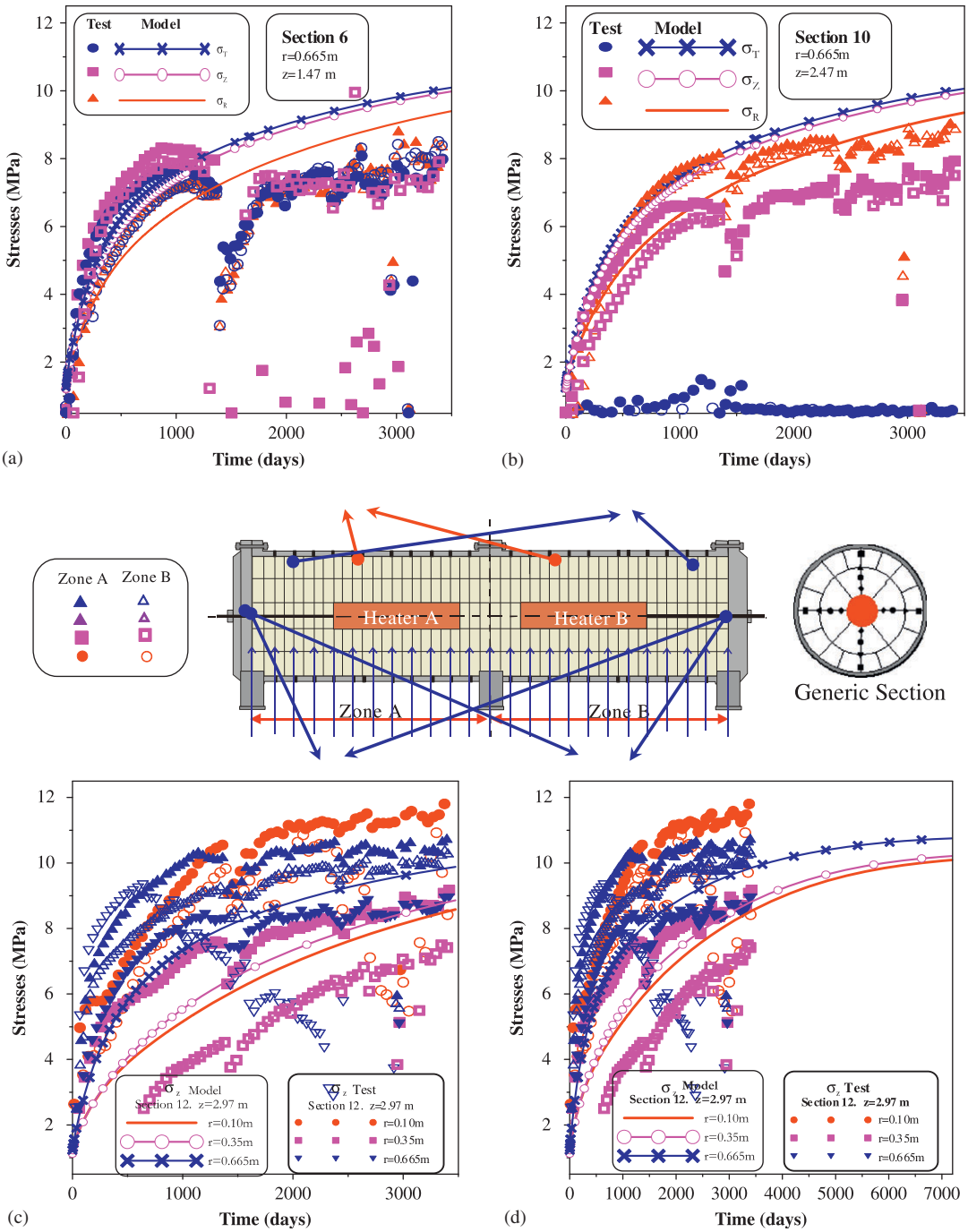

Figure 9. Evolution of stresses in the mock-up test. Observed versus computed values (OBC model). Bold symbols correspond to sensors in zone A, empty symbols correspond to sensors in zone B (Figure 2). (a) Sections A6–B6. (b) Sections A10–B10. (c) Sections A12–B12. (d) Long-term predictions.

thermal conductivity. Figures 7(c) and (d) present the long-term results, a slight increase of the temperature with saturation is predicted by the model.

Hydraulic results. Up to approximately day 900, the overall hydraulic behaviour of the test is closely reproduced by the model. As expected, an increasing saturation in zones close to the hydration boundary is observed whereas an initial intense drying in regions close to the heaters is

DOI: 10.1002/nag

followed by a slow hydration (Figure 8(a)). The close agreement of the observations from the two symmetric sections should be remarked. It is also interesting to note that zones close to a radius of 0.37 m show an initial temporary wetting, due to the condensation of the water vapour coming from the inner region of the barrier. This phenomenon is also reproduced by the model.

However, from about day 900, some differences are observed between model predictions and hydraulic behaviour of the test. The water entry calculated by the model moves progressively away predicting a faster hydration of the barrier (Figure 6(c)). This tendency can be clearly observed in terms of the rate of water intake; the experimental values undergo an important reduction in comparison with the results of the OBC model after 900 days. As for the evolution of relative humidity in sections involving heaters (e.g. Sections A4 and B4, Figure 8(a)) a significant reduction in the rate of relative humidity increase can be observed. Close to day 1381, some abnormal observations are obtained; they are due to an accidental overheating event that was quickly overcome. This episode is explained in detail in [13]. It seems that the transient period induced by the overheating was practically finished after day 1700; and the tendency to a slowing down of the barrier hydration is again recovered from that date on.

The hydraulic behaviour in the 'cool section' is quite different (Figures 8(b) and (d)). Now, a steady increase of hydration is observed and computed at all points, no noticeable drying occurs anywhere in the section. Again, the model results are initially very close to the observations. In this case, however, the slight departure of computations from the observations occurs at a significantly later date.

Mechanical results. Figure 9 presents the time evolution of stresses in selected positions of the barrier, according to the following convention: P_T, P_Z and P_R stand for tangential, longitudinal and radial stresses, respectively. A lesser repeatability of the observations can be observed, as it is often the case when dealing with stress measurements. It is also apparent that some sensors are malfunctioning.

Similar trends to those noted in the hydraulic problem are observed in the mechanical problem. Up to day 900 approximately, there is a good agreement between predictions and observations in sections close to the heater (Figures 9(a) and 8(b)). From that moment on, measured stresses respond to the slowing down of hydration, and a tendency to maintain constant values of stresses can be observed.

The overheating episode had different influences on the mechanical behaviour depending on the sections considered. In sections away from the heaters, the values and tendency registered prior to this event are recovered practically immediately (Figures 9(c) and (d)), whereas in sections close to the heaters, a more marked influence on the evolution of the stress field can be observed (Figures 9(a) and 8(b)). In those sections, the tendency to maintain a practically constant stress level (observed previous to this episode) has been recovered after the overheating event. But, the stresses are now lower compared with the ones measured before this event. This phenomenon has been explained using double structure concepts [13]. The overheating event has no perceptible effects in the 'cool' zones close to the ends of the experiment and the model captures well the measured values of stresses (Figure 9(c)). The long-term analysis predicts a maximum stress of the order of 10 MPa (Figure 9(c)).

In summary, thermal observations are generally well described by the model. However, the OBC analysis, while also reproducing successfully the initial hydration of the barrier, exhibits significant discrepancies concerning the long-term behaviour. This implies that the time for full saturation is severely underestimated. Owing to the hydro-mechanical coupling of the problem, stresses in the heater sections tend to be overestimated.

5. NUMERICAL ANALYSIS USING A DOUBLE STRUCTURE MODEL

5.1. Introduction

The understanding and the explanation of the apparent decay in the rate of the barrier hydration are key aspects regarding the ability to achieve reliable long-term predictions. Several studies were

DOI: 10.1002/nag

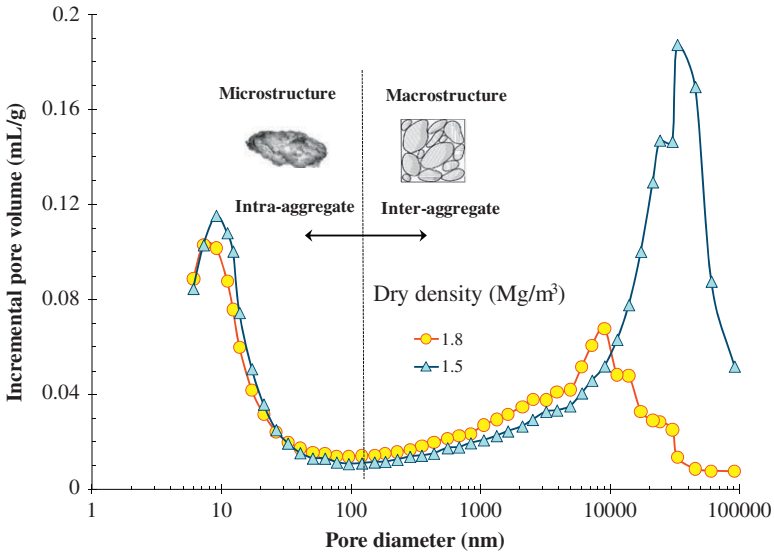

Figure 10. Distributions of incremental pore volume [21].

carried out to explore the possible phenomena that could cause the unexpected barrier behaviour. Initially it was examined whether, with minor modifications of the constitutive laws or their parameters, it was possible to explain and reproduce more closely the global and local evolution of the test. A wide-ranging sensitivity study was carried out to that end but it proved impossible to obtain a set of constitutive laws and materials parameters (with physical meaning) that led to predictions consistent with the observations [24]. Another uncertainty concerned whether the experiment was airtight or not. Hence analyses were carried out considering the two extreme conditions: free flow of air in and out of the experiment or a completely airtight experiment. Practically no influence on the results has been observed in relation to this condition. The hydration system of the experiment was also examined to discard the possibility that the water supply to the barrier was altered. It was experimentally confirmed that there was no obstruction in the hydration system or geotextile and that the water intake was nearly uniform over the entire hydration front. Support for the fact that the observed slowing down of hydration was genuine was provided by similar observations in other experiments. For instance, a lower level of saturation, compared with the expected one, has been observed in the large-scale ITT test performed in the Canadian underground laboratory near Winnipeg [32, 33]. Thomas *et al.* [33] concluded that 'standard THM models' were not able to capture the slow hydration observed in the experiment. Similar trends have been observed in other heating and hydration experiments involving expansive clays, as for example in the thermo-hydraulic cells that are being used at CIEMAT facilities.

An aspect that had not been considered in the formulation used hitherto and that may have a significant effect on predictions is the evolving nature of the fabric and microstructure of the compacted bentonite during hydration. Incorporation of this feature requires, however, the use of more advanced models as described below.

5.2. *Fabric of FEBEX bentonite*

Mercury intrusion porosimetry (MIP) tests were performed to examine the pore size distribution of statically compacted samples of FEBEX bentonite [23]. Figure 10 shows the measured incremental pore volume for two samples compacted to very different values of dry density (ρ_d), 1.5 and 1.8 Mg/m^3. It can be observed that the pore size distribution is clearly bimodal, very characteristic of these types of materials [34]. The dominant values are 10 nm that would correspond to the pores inside clay aggregates (i.e. small 'intra-aggregate', or 'intra-pedal', pores that remain largely saturated), and a larger pore size that depends on the compaction dry density and ranges from 10 μm (for $\rho_d = 1.8$ Mg/m^3) to 40 μm (for $\rho_d = 1.5$ Mg/m^3). These larger voids would correspond

DOI: 10.1002/nag

to the 'inter-aggregate' (or 'inter-pedal') pores that may, or may not, be saturated but provide pathways for the movement of 'free water'. The boundary between the two pore size families can be seen to be around 0.13 μm, as pores smaller than this size do not appear to be affected by the magnitude of the compaction load. This double structure has also been detected using other techniques, such as SEM (Scanning Electron Microscope) and water retention curve tests [23]. The two dominant pore sizes could be associated with two basic structural levels (Figure 10): (i) the macrostructure, associated with the global arrangements of clay aggregates (the skeleton of the material), with macropores between them and (ii) the microstructure, which corresponds to the active clay minerals and their vicinity. Evidently, the microstructure organization of expansive clays is very complex and more pore levels could be distinguished [35–37]. However, for the sake of simplicity, only the two basic structural levels identified above are considered. The approach could in fact be extended to include more structural levels in the analysis, if it is deemed relevant.

During hydration the fabric of expansive clays is not static but evolving. A systematic study was performed using ESEM (Environmental Scanning Electron Microscope) and SEM techniques to analyse the fabric changes of FEBEX bentonite during progressive wetting [29]. Suction changes under isochoric conditions were applied to samples before the observations. Figure 11 presents images taken at different suctions for a bentonite with a dry density around 1.40 mg/m^3. The differences in the final dry density are due to the rebound experienced by the bentonite after unloading. Although these tests provide mainly qualitative information, they clearly show the progressive occlusion of the inter-aggregate pores (macropores) due to swelling of active clay particles (microstructure).

5.3. Mechanical model

Based on the general framework for expansive soils proposed by Gens and Alonso [38] a double structure model has been proposed to describe the behaviour of swelling materials. The model explicitly considers the two dominant levels of pore sizes actually present in compacted expansive clays. The distinction between macro- and microstructure provides the opportunity to take into account the dominant phenomena that affect the behaviour of each structural level and the main interactions between them. The capabilities of the double structure model to reproduce and predict the mechanical behaviour of FEBEX bentonite under different stress paths involving loading, suction and temperature changes have been demonstrated elsewhere [13, 14, 23, 39, 40]. In spite of the complexity observed in those tests (i.e. yield phenomena, dependency of swelling strains on applied stresses, stress path dependency of strains and peaks in the swelling pressure tests), a good reproduction of the behaviour of the compacted bentonite has been achieved.

The complete definition of the double structure model requires the proposal of laws to describe (i) the macrostructural level, (ii) the microstructural level and (iii) the coupling between both structural levels. The double structure model has been described in detail elsewhere [13, 14] and only a brief summary of its main features are presented herein.

Macrostructural model. The inclusion of the macrostructural level in the analysis allows the consideration of phenomena that affect the skeleton of the material (i.e. inter-pedal behaviour), for instance yielding due to loading and wetting. The original version of the BBM for non-expansive materials (i.e. $\alpha_s = 0$ and $\alpha_{sp} = 0$, in Equations (9a) and (9b)) has been adopted to describe the macrostructural behaviour (Section 3.2).

Microstructural model. The microstructure is the seat of the basic physico-chemical phenomena occurring at clay particle level (i.e. intra-pedal behaviour). The strains arising from microstructural phenomena are considered non-linear elastic and, for simplicity, volumetric [13, 38]. The microstructural strains are proportional to the microstructural effective stress ($\hat{p}$) through a microstructural bulk modulus according to

$$\hat{p} = p + \chi(s + s_o) \quad \text{(a)}; \qquad \dot{\varepsilon}_{vm} = \frac{\dot{\hat{p}}}{K_m} = \frac{\dot{p}}{K_m} + \chi\frac{\dot{s}}{K_m} \quad \text{(b)} \tag{20}$$

DOI: 10.1002/nag

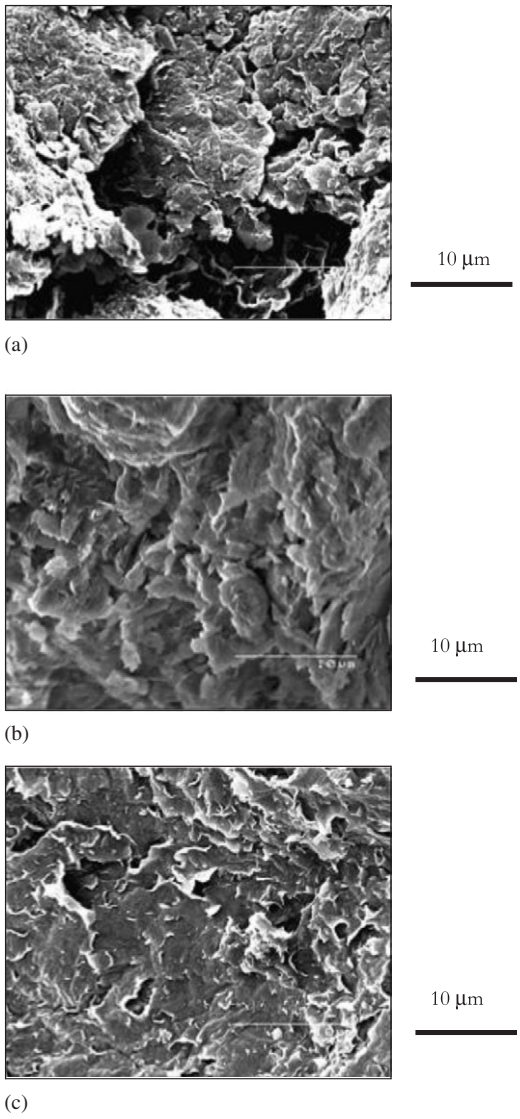

Figure 11. ESEM analysis of compacted FEBEX bentonite [27]. (a) Sample with hygroscopic water content ($\rho_d = 1.40\,mg/m^3$). (b) Sample after application of a suction of 10 MPa in isochoric (constant volume) conditions (ρ_d final $= 1.46\,mg/m^3$) on bentonite initially compacted in hygroscopic conditions ($\rho_d = 1.65\,mg/m^3$). (c) Sample after saturation in isochoric conditions (ρ_d final $= 1.43\,mg/m^3$) on bentonite initially compacted with hygroscopic water content to $\rho_d = 1.65\,mg/m^3$.

where the subscript 'm' refers to the microstructural level, the subscript 'v' refers to the volumetric component of the strains; p is the net mean stress, s_o the osmotic suction and $(s+s_o)$ is the total suction. The parameter χ was originally included (e.g. [41]) to account for the possibility that the microstructure may become unsaturated. For example, Alonso [41] suggests that χ is proportional to the degree of saturation through the following expression: $\chi(S_l)^n$; where n is a coefficient. Herein it has been assumed that $\chi = 1$. Under this condition, the mean effective stress controls the mechanical behaviour at the microstructural level [38].

In this work it is also assumed that the total suction is equal to the matric suction because the effect of the osmotic suction is not considered in this analysis. Recently, the expansive model has been extended to include geochemical variables such as osmotic suction and cation exchange [42]. K_m is the microstructural bulk modulus. As explained in Gens and Alonso [38], any elastic

DOI: 10.1002/nag

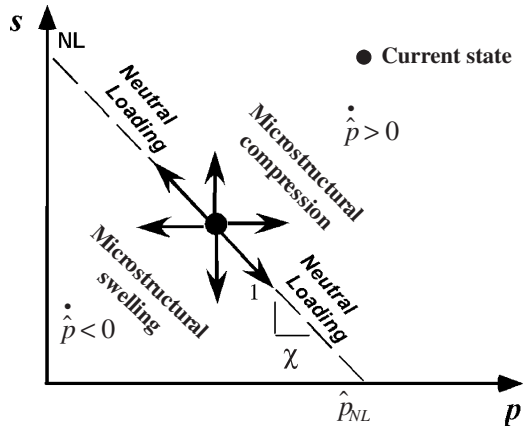

Figure 12. Definition of microstructural swelling and contraction directions.

model able to describe the behaviour of active clay particles can be adopted for the microstructural law. In this work the exponential type model suggested by Alonso [41] has been adopted (see Equation A6 in the Appendix). The model has its roots in the exponential type model describing the clay interlayer distance as a function of effective stress in double layer theories [41]. Hydraulic equilibrium is assumed between the water potentials of both structural levels, the extension to non-equilibrium conditions is presented elsewhere [31, 41, 42].

The concept of a Neutral Line (NL) is introduced corresponding to constant $\hat{p}$ and no microstructural deformation (Figure 12). The NL divides the $p-s$ plane into two parts, defining two main generalized stress paths, which are identified as MC (microstructural contraction) when there is an increase in $\hat{p}$ and MS (microstructural swelling) in the opposite case [13].

Interaction between macro- and microstructure. Based on experimental evidence, it is assumed that the macrostructure is affected by microstructural deformations potentially in an irreversible way [38]. A hypothesis of the model is that the plastic deformations of the macrostructure induced by microstructural effects ($\dot{\varepsilon}^{p}_{vM\to m}$) are proportional (see Equation (21a)) to the microstructural strains (ε_{vm}) according to interaction functions f [13, 38]. Two interaction functions f are defined: f_c for microstructural contraction paths and f_S for microstructural swelling paths. The interaction functions depend on the ratio p/p_0. This ratio is a measure of the degree of openness of the macrostructure relative to the applied stress state [38]. The functions adopted in this analysis are introduced in the Appendix (A9) and (A10).

The total plastic macrostructural strains ($\dot{\varepsilon}^{p}_{v}$) are obtained (see Equation (21b)) as the sum of the plastic deformations induced when yielding of the macrostructure takes place (evaluated from (6)), and the inelastic strains induced by the microstructure through the interaction mechanism [13] (calculated through 21(a)). This can be expressed mathematically as follows:

$$\dot{\varepsilon}^{p}_{vM\to m} = f\dot{\varepsilon}_{vm} \quad (a); \qquad \dot{\varepsilon}^{p}_{v} = \dot{\varepsilon}^{p}_{vLC} + \dot{\varepsilon}^{p}_{vM\to m} \quad (b) \tag{21}$$

The coupling between macro and micro levels is given by p_0^* (the hardening variable of the macrostructure, Figure 3), which depends on the total plastic volumetric strain (7). In this way it is considered that the microstructural changes can affect the global arrangements of clay aggregates. More details about the interaction between the two structural levels are presented elsewhere [13, 14, 23, 41].

The experimental validation of the double structure model using experimental data of FEBEX bentonite was presented in [23]. The main model parameters are presented in Table III. The dry density of these tests was $1.70\,mg/m^3$, whereas the global dry density of the mock-up test is $1.65\,mg/m^3$. In order to take into account this difference in dry density, the pre-consolidation stress has been modified [38]. As mentioned above, p/p_0 is a measure of the degree of openness

DOI: 10.1002/nag

Table III. Parameters used to define the elasto-plastic constitutive law.

Parameters defining the Barcelona Basic Model for macrostructural behaviour							
κ	κ_s	$\lambda_{(o)}$	p_c (MPa)	r	ζ (MPa^{-1})	p_0^* (MPa)	α_0 ($^\circ$C^{-1})
0.005	0.001	0.080	0.50	0.90	0.2	5.4	$1.0\,e^{-5}$
Parameters defining the law for microstructural behaviour							
α_m (MPa^{-1})			β_m (MPa^{-1})			χ	
$2.0\,e^{-02}$			$2.1e^{-03}$			1	
Interactions functions							
$f_C = 1 + 0.9\tanh(20(p/p_0) - 0.25)$;						$f_S = 0.8 - 1.1\tanh(20(p/p_0) - 0.25)$	
e_{macro}						e_{micro}	
0.20						0.45	

of the macrostructure [13, 17] (e.g. a low ratio implies a dense packing). Therefore, the effect of the soil density can be modelled considering that the higher the soil density (for a given suction), the higher the p_0. A value of 7.5 MPa has been adopted for p_0, which implies (according to the adopted LC curve) a value of 5.4 MPa for the saturated pre-consolidation stress.

5.4. Hydraulic behaviour

There is a strong interaction between the active clay particles and the water present in their vicinity. Apart from the free water, the rest of the water in clay is affected by psycho-chemical phenomena occurring at clay particle level. For example, a noticeable variation of the water viscosity (up to a factor of 7 for positions close to active clay particles) was estimated by molecular dynamic simulations [44]. The interlamellar water is strongly attached to the clay surfaces and it has been considered as practically immobile water under normal environmental loads by some authors (i.e. [45]). On the other hand, the properties of the intra-aggregate water will depend on its proximity to the clay particle face [46]. Based on these ideas, in this section it is assumed that the macropores are the main paths for the movement of water due to advection.

In classical (or conventional) flow models, as the one presented in Section 3.2, the dependence of permeability on the pore structure is introduced through a relationship between permeability and total porosity (12). Considering that the macroporosity (i.e. volume of macro-voids divided by the total volume) is the void fraction that has the main influence on the water movement due to hydraulic gradient, it seems more appropriate to relate the intrinsic permeability in terms of macropore changes. An advantage of the double structure model [13] is that as the two pore levels are explicitly considered in the analysis, the evolution of macro- and microporosity can be tracked and then they can be used to update the permeability field. In this work it is suggested that the intrinsic permeability is simply a function of the macroporosity through an exponential law (22), as follows:

$$\mathbf{k} = k_0 \exp[b(\phi_M - \phi_{M0})]\mathbf{I} \tag{22}$$

where ϕ_M is the macroporosity, k_0 is the intrinsic permeability at a reference porosity (ϕ_{M0}), b is a model parameter and $\boldsymbol{I}$ is the identity tensor. The model parameters adopted in the analysis ($k_0 = 5.0 \times 10^{-20}\,m^2$; $\phi_{M0} = 0.14$ and $b = 50$) have been determined from back-calculating the results of permeability tests performed under conditions of constant volume [31]. For this purpose, a series of numerical simulations of the permeability tests at different initial dry densities have been carried out solving them as a boundary value problem using the double structure model in the simulations. Figure 13 presents the measured saturated permeability of FEBEX bentonite at different densities together with the results obtained in the simulation using the exponential model (22).

DOI: 10.1002/nag

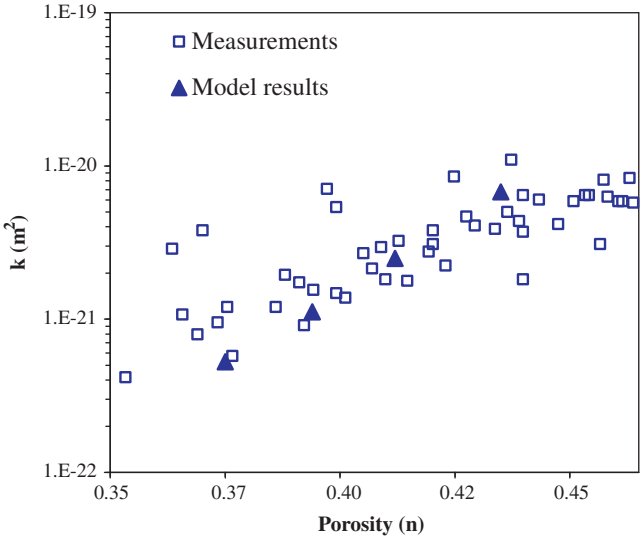

Figure 13. Measured saturated water permeability of FEBEX betonite [1], together with model results obtained after modelling of permeability tests a boundary value problem with the double structure model.

5.5. Numerical results

The double structure models for the mechanical and hydraulic problem presented above (Sections 5.3 and 5.4) have been used in a new analysis of the THM behaviour of the clay barrier. All the other constitutive laws defined in Section 3.2 have been left unchanged in the analysis (i.e. the same retention curve and thermal conductive laws, Figures 4(b) and (d) respectively, have been adopted). Also, the same initial and boundary conditions adopted for the 'OBC' model (Section 4) have been prescribed for the hydraulic, mechanical and thermal problems.

Figure 14 presents the evolution of temperature for the two representative sections analysed. The computed values obtained with the double structure model are coded as 'Dou', whereas the results of the conventional model (OBC) are also provided for comparison. As expected, the temperature field is also well captured by this model. Figures 15(a) and (b) present the results of relative humidity in a 'hot cross section' and a 'cold cross section', respectively. Concerning the evolution of the relative humidity in the section involving heaters (Figure 15(a)), it can be observed that the model can now capture it quite well, especially in the inner zones ($r = 0.22$ m and $r = 0.37$ m) where discrepancies were larger. No significant differences between the two analyses are obtained in the cold cross section (Figure 15(b)). It can also be observed that the new model captures the hydro-mechanical coupling of this problem (Figure 15(c)), reproducing the clear tendency to maintain a practically constant value of the stress level (close to 7 MPa in the test). Regarding water intake (Figure 15(d)), the response of the model is very satisfactory, especially when compared with the measurements and the OBC model.

The analysis of the distribution of some relevant variables along the barrier computed for different times can contribute to a deeper insight into the problem. Figures 16(a)–(d) present the computed distributions of macro-, micro- and global void ratios, and also of the degree of saturation at different times for the 'hot section'. It can be noted that the microstructure expands in the external zones due to hydration and it contracts in zones close to the heater due to strong drying. The front of the swelled microstructure advances progressively towards the inside of the barrier as the experiment progresses. As for the macropores, a swelling behaviour can be seen but only at the beginning of the test and for a very thin zone close to the hydration front. This is due not only to suction reduction but also to the interaction mechanism between the two structural levels (a detailed explanation of the different plastic mechanisms of the model during the heating and hydration of the barrier is presented in [14]). For other times and positions the values of

DOI: 10.1002/nag

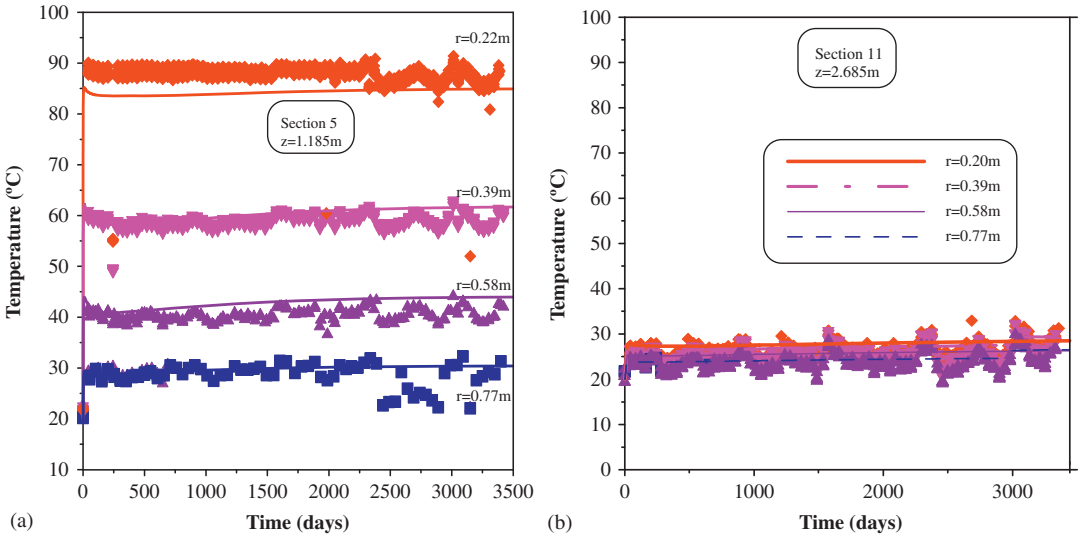

Figure 14. Observed temperature versus computed values using 'Dou' model: (a) Section A5 and (b) Section A11.

macro void ratio are lower than the initial ones. This is caused by the fact, already mentioned, of microstructural expansions under conditions of practically constant volume. The final condition corresponds to significant reductions of the macropores across the barrier, which is more marked in the external zones of the barrier. Macrostructural compression (collapse) can also be observed along the barrier moving progressively to more internal zones as hydration goes on. It can be observed that zones close to a radius of 0.35 m are strongly affected by the condensation of water vapour coming from the inner region of the barrier. This local wetting also induces a marked macro-void reduction in this region. Regarding the degree of saturation, it can be noted that the shape of the hydration front is very similar to that of the microstructural void ratio. This result is in agreement with the adopted conceptual model, which considers that a larger amount of water is stored in the microstructure. The global void ratio is greater in the outer zones of the barrier and lower in the inner regions. In that sense, the model reproduces a reduction in clay densities in zones close to the hydration front, as saturation progresses. The key point is, however, that using in this approach under constant volume conditions, the reduction in clay density is associated with a reduction of the volume of the macropores available for water flow.

A better understanding of the differences between the two models on the predicted hydration process can be achieved by observing the predicted evolution of porosities and their impact on intrinsic permeability. Figure 17(a) shows the evolution of porosity for two extreme radii computed using the 'OBC' model. Through (12), higher permeabilities are computed in zones close to the hydration front (associated with lower densities), and lower permeabilities in more internal zones. Figure 17(b) presents, for the same radii, the evolution of the macroporosity. As can be observed, in this model the response is quite different, with a tendency to reduce the macroporosity in both locations and, consequently, to reduce also the associated intrinsic permeability. A more external radius ($r = 0.75$ m) is also included in the figure, it can be seen that this effect is even more significant in zones near the hydration front. The break observed in Figure 17(b) for a radius of 0.70 m close to the day 1400 of the test is due to macrostructural collapse [14]. According to this simulation, as the barrier is hydrated the pores available to the liquid flow suffer a progressive reduction, due mainly to microstructure swelling under confined conditions. This is in agreement with the experimental behaviour observed in Figure 11. As a consequence, the full saturation of the barrier is delayed. The consequence of this hydration-locking is quite evident in zones close to the heater; the decrease of the permeability in the zones close to the hydration front reduces the supply of liquid flow to the internal zones which are subjected to the heater-induced drying. The

DOI: 10.1002/nag

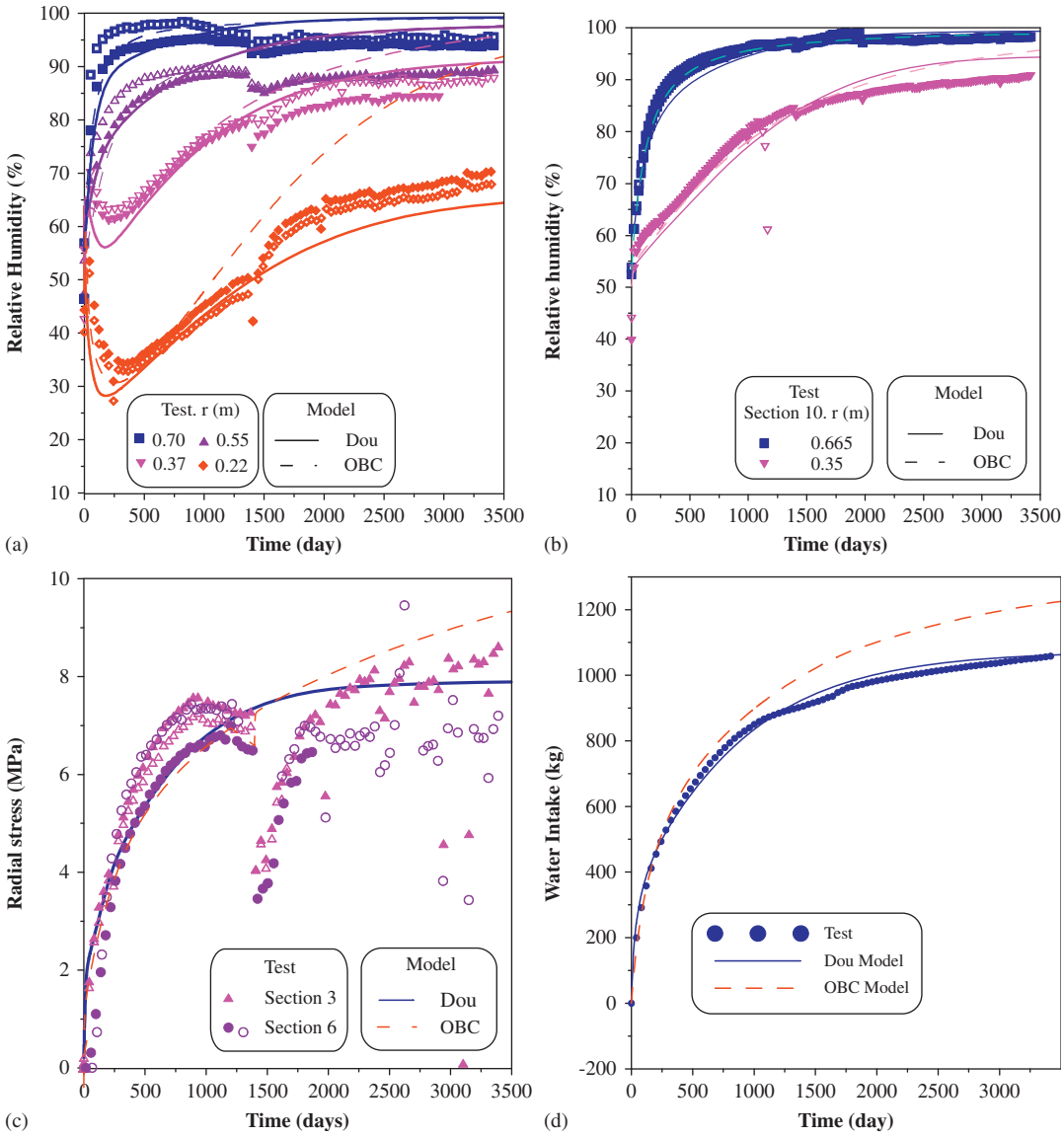

Figure 15. Observed versus computed values of 'Dou' and 'OBC' models: (a) relative humidity (Sections A4–B4); (b) relative humidity (Sections A10–B10); (c) radial stress (Sections A3–B3 & A6–B6); and (d) water intake.

final outcome is that hydration slows down dramatically, leaving an important zone of the barrier in unsaturated conditions.

The differences between the predictions of the two models (OBC and Dou) are even more evident when the long-term predictions are analysed. Figure 18 shows the comparisons between the long-term predictions of both models (alongside the experimental data) in terms of relative humidity and water intake. The double structure model is able to simulate the type of hydration locking observed in the test. As can be observed, significant zones of the barrier may remain in a non-saturated condition for a considerable period of time. This is qualitatively in agreement with the tendency observed in the barrier up to the present date.

It is possible that other physical and chemical phenomena could have an influence on the slow hydration observed in the clay barrier [47]. Other alternative phenomena are being explored to explain the behaviour of the mock-up test, as for example, the effect of a threshold gradient in the permeability law and the influence of thermo-osmotic flow on the kinetic of the barrier hydration.

DOI: 10.1002/nag

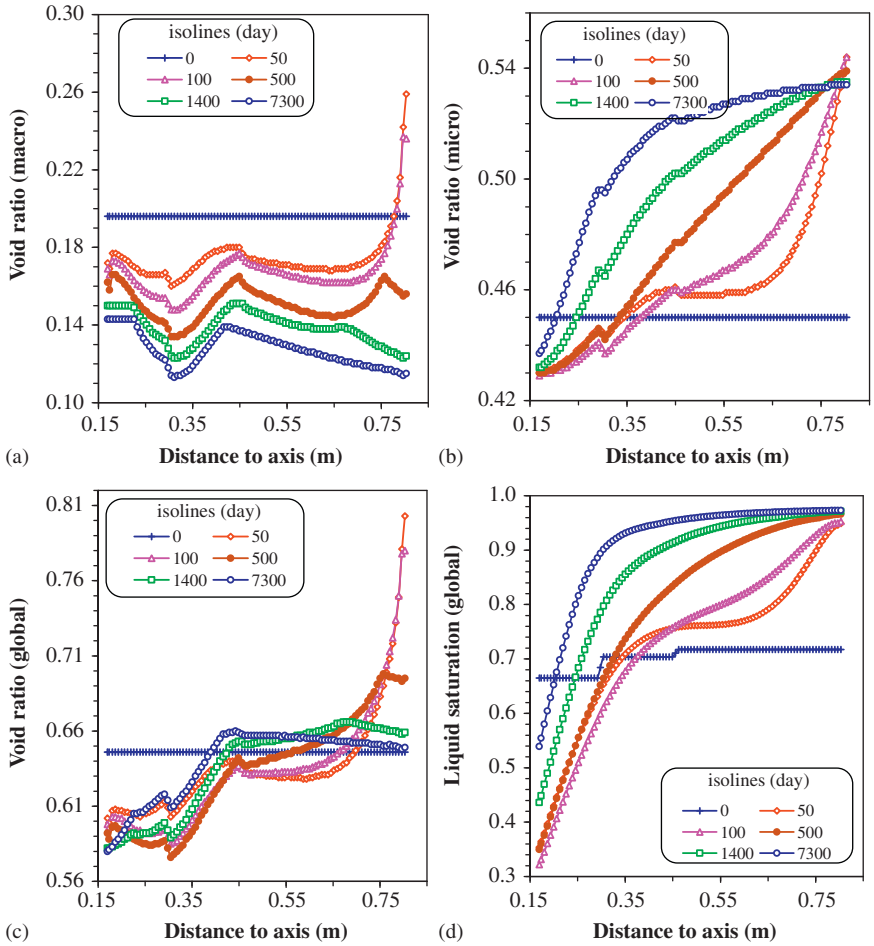

Figure 16. Hot cross section: isolines of macro void ratio (a); micro void ratio (b); global void ratio (c) and (d) liquid saturation.

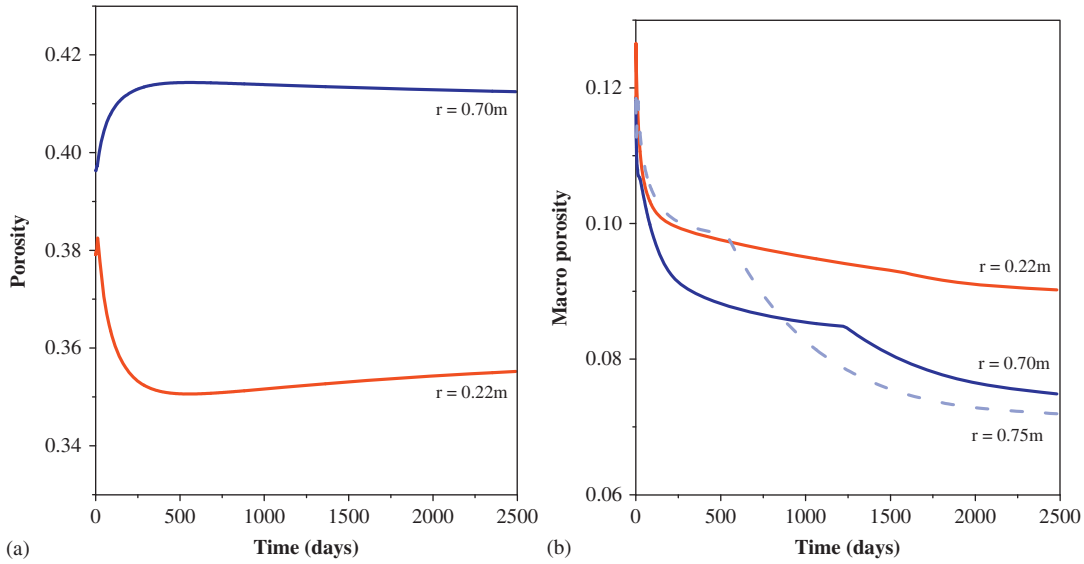

Figure 17. Sections A4–B4: computed evolution for two extreme radii of (a) porosity by using the 'OBC' model and (b) macroporosity by using the 'Dou' model.

DOI: 10.1002/nag

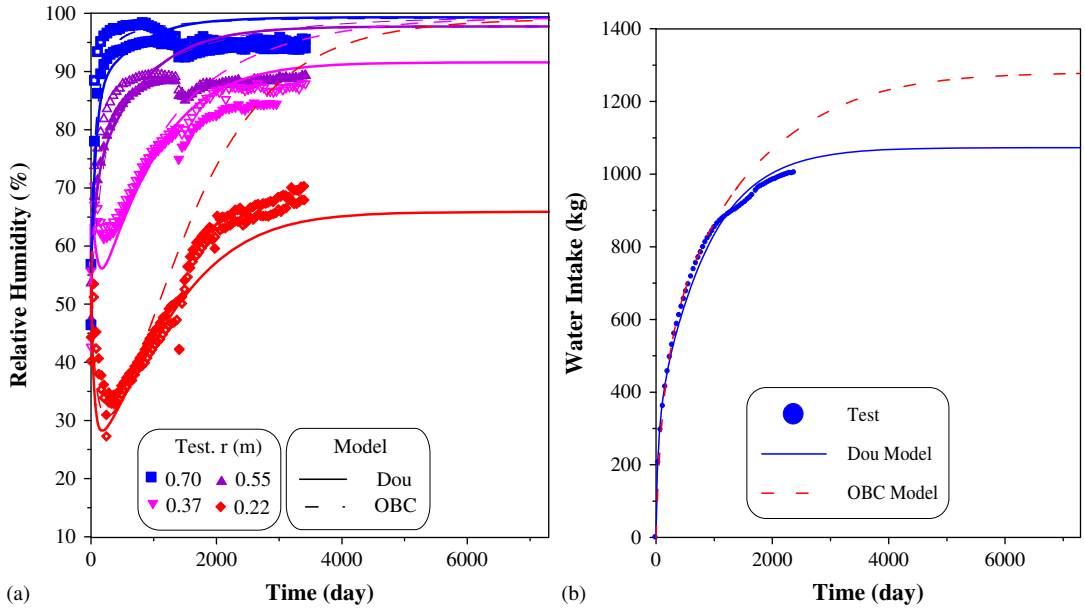

Figure 18. Long-term predictions of 'Dou' and 'OBC' models for (a) relative humidity and (b) water intake.

Finally, it is important to bear in mind that there is an important difference between the test and a radioactive waste disposal site. In the experiment, the temperature is maintained constant at the contact between heater and bentonite (equal to 100°C) but, under real repository conditions, the waste temperature will reduce progressively as the time goes on, altering the kinetics of the hydration process.

6. CONCLUSIONS

In this paper the analysis of a large-scale heating at almost full scale, performed under well-controlled THM conditions has been described. The 'OBC' model presented in the first part of the paper was formulated using a fully coupled THM approach for a single porosity medium, in which all the basic processes and couplings deemed relevant were considered. Extensive laboratory work carried out in the context of the FEBEX project allowed the identification of the main models parameters required for the THM model. In spite of a very successful modelling of the early transient THM behaviour, the results obtained with this model are not totally satisfactory, because the simulation overpredicts the long-term hydration rate of the barrier. Comparing experimental data versus model results, a slowing down in the hydration kinetics of the test with respect to model predictions can be observed after about three years of testing. A tendency to maintain a constant and very low rate of water intake and nearly constant values of the main variables (relative humidity and stresses) at different radii of the barrier was particularly observed in the cross sections involving heaters. Changes in the constitutive law or their parameters could not reproduce accurately the test evolution. The conventional THM model used in the numerical analysis predicts a progressive increment of the water permeability in external zones of the barrier as saturation goes on, due to two main reasons: (a) increases of the relative permeability due to increasing degree of saturation and (b) swelling of the expansive clay (with the corresponding increase of porosity). Although the slow hydration and extended unsaturation will be beneficial to the long-term storage of fuel waste, it is crucial to investigate the source of this unexpected barrier behaviour. Experimental evidence indicates that the behaviour of expansive clays under confined hydration is more complex. A progressive occlusion of the macropores has been observed in the laboratory leading to potentially large reductions in intrinsic permeability.

DOI: 10.1002/nag

Consequently, a double structure framework has been used to simulate the THM behaviour of the test. The explicit consideration of the two structural levels provides the opportunity to define the constitutive laws and properties of the two pore levels that actually exist in the compacted FEBEX bentonite. The inclusion in the modelling of the changes in the clay fabric (through the double structure approach) has allowed a more detailed analysis of the barrier behaviour. In this model the evolution of the clay fabric (macro- and microporosity) is controlled by the changes in the main variables of the problem (displacements, temperature and suction), which are considered in a fully coupled way. In this context, the main phenomena that affect the changes in both pore levels, and their mutual interactions, are taken into account.

According to the model results, as the barrier hydration progresses, the macropores available to the liquid flow suffer a progressive reduction. This is due mainly to microstructural swelling under confined conditions. As a consequence, the full saturation of the barrier is drastically delayed. This phenomenon affects especially the zones close to the heater, because the reduction of the permeability in the zones close to the hydration front reduces the liquid flow supply to the internal zones which have been subjected to heating-induced drying.

In summary, the use of the double structure approach has allowed the adoption of a conceptual model for the hydration of the swelling clays closer to the actual behaviour of expansive clays under confined conditions. The model has also contributed to a better understanding of the complex behaviour observed in this large-scale heating test and has provided a physically based explanation for the very slow hydration of the barrier.

APPENDIX A

Mechanical constitutive model

The BBM yield surface (F_{LC}) is given by (4) and the plastic potential (G) is expressed as

$$G=\alpha_G 3J^2-\left[\frac{g(\theta)}{g(-30^\circ)}\right]^2 M^2(p+p_s)(p_0-p)=0 \tag{A1}$$

where α_G is determined according to [17]. The dependence of the tensile strength on suction and temperature is given by

$$p_s=ks\mathrm{e}^{-\rho\Delta T} \tag{A2}$$

where k and ρ are model parameters [18]. The dependence of p_0 on suction is given by

$$p_0=p_c\left(\frac{p_{0T}^*}{p_c}\right)^{\frac{\lambda_{(0)}-\kappa}{\lambda_{(s)}-\kappa}}(a);\quad p_{0T}^*=p_0^*+2(\alpha_1\Delta T+\alpha_3\Delta T|\Delta T|)(b) \tag{A3}$$

where p_c is a reference stress, α_1 and α_3 are models parameters [18]. $\lambda_{(s)}$ is the compressibility parameter for changes in net mean stress for virgin states of the soil. This parameter depends on suction according to

$$\lambda_{(s)}=\lambda_{(0)}[r+(1-r)\exp(-\zeta s)] \tag{A4}$$

where r is a parameter which defines the minimum soil compressibility (at infinite suction) and ζ is a parameter which controls the rate of decrease of soil compressibility with suction [17].

The macrostructural bulk modulus (K) for changes in mean stress is evaluated with the following law:

$$K=\frac{(1+e)}{\kappa}p \tag{A5}$$

where κ is evaluated according to (9).

DOI: 10.1002/nag

The microstructural bulk modulus (K_m) is calculated as follows [41]:

$$K_m = \frac{e^{-\alpha_m \hat{p}}}{\beta_m} \tag{A6}$$

where α_m and β_m are model parameters. The macrostructural bulk modulus for changes in suction is computed considering the following law:

$$K_s = \frac{(1+e_M)(s+p_{atm})}{\kappa_s} \tag{A7}$$

The macrostructural bulk modulus for changes in suction is computed considering the following law:

$$K_T = \frac{1}{(\alpha_0 + \alpha_2 \Delta T)} \tag{A8}$$

where α_0 and α_2 are parameters related to the elastic thermal strain [18].

The double structure model require the definition of the interaction functions [13, 14, 23, 38, 41]. The interaction functions presented below have been adopted in this work. More details about these particular functions are presented in [23].

$$f_C = 1 + 0.9 \tanh(20(p/p_0) - 0.25) \tag{A9}$$

$$f_S = 0.8 - 1.1 \tanh(20(p/p_0) - 0.25) \tag{A10}$$

The stress invariants are defined as follows:

$$p = \left(\frac{1}{3}\right)(\sigma_x + \sigma_y + \sigma_z) \tag{A11}$$

$$J^2 = 1/2 \text{trace}\,(s^2) \tag{A12}$$

$$\theta = -\frac{1}{3}\sin^{-1}(1.5\sqrt{3}\,\det s/J^3) \tag{A13}$$

being

$$\mathbf{s} = \boldsymbol{\sigma} - p\mathbf{I} \tag{A14}$$

where $\boldsymbol{I}$ is the identity tensor.

ACKNOWLEDGEMENTS

The authors acknowledge ENRESA for funding this work. The experimental and numerical work was also funded by the European Commission through the FEBEX I, FEBEX II and NF-PRO projects. The support of the Ministry of Education of Spain through research grant BIA2008-06537 is gratefully acknowledged.

REFERENCES

1. Huertas F, Farina P, Farias J, Garcia-Sineriz JL, Villar MV, Fernandez AM, Martin PL, Elorza FJ, Gens A, Sanchez M, Lloret A, Samper J, Martinez MA. Full-scale engineered barrier experiment. *Updated Final Report*, *Technical Publication 05-0/2006*, Enresa, Madrid, 2006.
2. Volckaert G, Dereeper B, Put M, Ortiz L, Gens A, Vaunat J, Villar MV, Martin PL, Imbert C, Lassabatère T, Mouche E, Cany F. A large-scale in situ demonstration test for repository sealing in an argillaceous host rock. Reseal *Phase I Project Report*, European Commission, Brussels, 2000.
3. Dixon D, Chandler N, Graham J, Gray M. Two large-scale sealing tests conducted at Atomic Energy of Canada's underground research laboratory: the buffer-container experiment and the isothermal test. *Canadian Geotechnical Journal* 2002; **39**:503–518.
4. Svemar C, Push R. Äspö Hard Rock Laboratory. *International Progress Report* 2002; IPR-00-30, SKB.

DOI: 10.1002/nag

5. Gens A, Sánchez M, Guimaraes L, Alonso E, Lloret A, Olivella S, Villar MV, Huertas F. A full scale in situ heating test for high level nuclear waste disposal. Observations analysis and interpretation. *Géotechnique* 2009; **59**:377–399. DOI: 10.1680/geot.2009.59.4.377.
6. Martin PL, Barcala JM. Large scale buffer material test: mock-up experiment at CIEMAT. *Engineering Geology* 2005; **81**(3):298–316.
7. Sneyers A, Grambow B, Hernán P, Hans-Joachim A, Aranyossy JF, Johnson L. The Integrated Project NF-PRO: recent advances in European research on the near-field system. *Proceedings of the 11th International Conference on Environmental Remediation and Radioactive Waste Management*, Bruges, Belgium, 2–6 September 2007.
8. Olivella S, Carrera J, Gens A, Alonso EE. Non-isothermal multiphase flow of brine and gas through saline media. *Transport in Porous Media* 1994; **15**:271–293.
9. Olivella S, Gens A, Carrera J, Alonso EE. Numerical formulation for a simulator (CODE-BRIGHT) for the coupled analysis of saline media. *Engineering Computations* 1996; **13**(7):87–112.
10. Dixon D, Graham J, Gray M. Hydraulic conductivity of clays in confined tests under low hydraulic gradients. *Canadian Geotechnical Journal* 1999; **36**:815–825.
11. Cui Y, Loiseau C, Delage P. Water transfer through a confined heavily compacted swelling soil. *Proceedings of the Sixth International Workshop on Key Issues in Waste Isolation Research*, Paris, 2001; 43–60.
12. Delage P, Marcial D, Cui YJ, Ruiz M. Ageing effects in a compacted bentonite: a microstructure approach. *Géotechnique* 2006; **56**(5):291–304.
13. Sánchez M, Gens A, Guimarães L, Olivella S. A double structure generalized plasticity model for expansive materials. *International Journal for Numerical and Analytical Methods in Geomechanics* 2005; **29**:751–787. DOI: 10.1002/nag.434.
14. Sánchez M, Gens A, Guimarães L, Olivella S. Implementation algorithm of a generalized plasticity model for swelling clays. *Computers and Geotechnics* 2008; **35**:860–871. DOI: 10.1016/j.compgeo.2008.08.004.
15. Siemens G, Blatz J. Evaluation of the influence of boundary confinement on the behaviour of unsaturated swelling clay soils. *Canadian Geotechnical Journal* 2009; **46**:339–356.
16. Gens A, Garcia Molina A, Olivella S, Alonso EE, Huertas F. Analysis of a full scale in-situ test simulating repository conditions. *International Journal for Numerical and Analytical Methods in Geomechanics* 1998; **22**:515–548.
17. Alonso E, Gens A, Josa A. A constitutive model for partially saturated soils. *Géotechnique* 1990; **40**(3):405–430.
18. Gens A. Constitutive laws. *Modern Issues in Non-Saturated Soils*. Springer: Berlin, 1995; 129–158.
19. Hueckel T, Baldi G. Thermoplasticity of saturated clays: experimental constitutive study. *Journal of Geotechnical Engineering* (ASCE) 1990; **116**(12):1778–1795.
20. Romero E, Gens A, Lloret A. Suction effects on a compacted clay under non-isothermal conditions. *Géotechnique* 2003; **53**(1):65–81.
21. Villar MV, Lloret A. Temperature influence on the hydro-mechanical behaviour of a compacted bentonite. *Workshop on Large Scale Field Tests in Granite*, Sitges, Spain, 2003; CD format.
22. CODE_BRIGHT User's Manual. Technical University of Catalonia, 2009.
23. Lloret A, Villar MV, Sánchez M, Gens A, Pintado X, Alonso EE. Mechanical behaviour of heavily compacted bentonite under high suction changes. *Géotechnique* 2003; **53**(1):27–40.
24. Sánchez M, Gens A. Second report on *THM* modelling results. FEBEX II. *ENRESA Report*: *70-UPC-L-5-011*, 2002.
25. Lloret A, Villar M. Variation of the intrinsic permeability of expansive clays upon saturation. In *Clay Science for Engineering*, Adachi K, Fukue M (eds). Balkema: Rotterdam, 2000; 259–266.
26. Olivella S, Gens A. Vapour transport in low permeability unsaturated soils with capillary effects. *Transport in Porous Media* 2000; **40**:219–241.
27. van Genuchten R. Calculating the unsaturated hydraulic permeability conductivity with a new closed-form analytical model. *Water Resource Research* 1978; **37**(11):21–28.
28. Fredlund D, Xing A. Equations for the soil-water characteristic curve. *Canadian Geotechnical Journal* 1994; **31**:521–532.
29. Villar MV, Martin P, Lloret A, Romero E. Final report on thermo-hydro-mechanical laboratory test. *FEBEX II. ENRESA Report*: *70-IMA-L-0-97*, 2004.
30. Hughes TJ. Generalization of selective integration procedures to anisotropic and nonlinear media. *International Journal for Numerical Methods in Engineering* 1980; **15**:1413–1418.
31. Sánchez M. Thermo-hydro-mechanical coupled analyses in low permeability media. *Ph.D. Thesis*, Universitat Politècnica de Catalunya, Spain, 2004.
32. Dixon D, Chandler N, Graham J, Gray M. Two large-scale sealing tests conducted at Atomic Energy of Canada's underground research laboratory: the buffer-container experiment and the isothermal test. *Canadian Geotechnical Journal* 2002; **39**:503–518.
33. Thomas H, Cleall P, Chandler N, Dixon D, Mitchell H. Water infiltration into a large-scale in-situ experiment in an underground research laboratory. *Géotechnique* 2003; **53**(2):207–224.
34. Alonso EE, Gens A, Hight DW. Special problem soils. General report. *Proceedings of the Ninth European Conference on SMFE*, Bruges, Belgium, vol. 3, 1987; 1146.
35. Push R, Karnland O. Physico/chemical stability of smectite clays. *Engineering Geology* 1996; **41**:73–85.
36. Saiyouri N, Hicher P, Tessier D. Microstructural approach and transfer water modelling in highly compacted unsaturated swelling clays. *Mechanics of Cohesive-Frictional Materials* 2000; **5**:41–60.

37. Hueckel T, Loret B, Gajo A. Expansive clays as two-phase deformable, reactive continua: concepts and modelling options. In *Chemo-mechanical Coupling in Clays*, Di Maio C, Hueckel T, Loret B (eds). Taylor and Francis: London, 2002; 105–121.
38. Gens A, Alonso EE. A framework for the behaviour of unsaturated expansive clays. *Canadian Geotechnical Journal* 1992; **29**:1013–1032.
39. Åkesson M, Jacinto A, Gatabin C, Sánchez M, Ledesma A. Bentonite THM behaviour under high temperature gradients. Experimental and numerical analysis. *Géotechnique* 2003; **59**(4):307–318. DOI: 10.1680/geot.2009.59.4.307.
40. Alonso E, Vaunat J, Gens A. Modelling the mechanical behaviour of expansive clays. *Engineering Geology* 1999; **54**:173–183.
41. Alonso E. Modelling expansive soil behaviour. *Second International Conference on Unsatured Soils*, Beijing, vol. 1, 1998; 37–70.
42. Guimarães L, Gens A, Sánchez M, Olivella S. Coupled THMC modelling of unsaturated swelling clays: constitutive formulation and boundary value problems Keynote paper. *Fourth Asian Pacific Conference on Unsaturated Soils*, Newcastle, Australia, vol. 2, 2010; 515–529.
43. Gens A, Vallejan B, Sánchez M, Imbert C, Villar MV, Van Geet M. Hydromechanical behaviour of a heterogeneous compacted soil: experimental observations and modelling. *Géotechnique* 2011; DOI: 10.1680/geot.2011.61.00.1.
44. Ichikawa Y, Kawamura K, Fujii N, Theramast N. Molecular dynamics and multiscale homogenization analysis of seepage/diffusion problem in bentonite clay. *International Journal for Numerical Methods in Engineering* 2002; **54**:1717–1749.
45. Hueckel T. Water-mineral interaction in hydromechanics of clay exposed to environmental loads: a mixture-theory approach. *Canadian Geotechnical Journal* 1992; **29**:1071–1086.
46. Mitchell J. *Fundamentals of Soil Behaviour* (2nd edn). Wiley: New York, 1993.
47. Gens A. Soil–environment interactions in geotechnical engineering. *Géotechnique* 2010; **60**(1):3–74. DOI: 10.1680/geot.9.P.109.